

Quantum advantages in timekeeping: dimensional advantage, entropic advantage and how to realise them via Berry phases and ultra-regular spontaneous emission

Arman Pour Tak Dost

Institute for Theoretical Physics, ETH Zurich, Switzerland

Mischa P. Woods*

*University Grenoble Alpes, Inria, Grenoble, France and
Institute for Theoretical Physics, ETH Zurich, Switzerland*

(Dated: March 20, 2023)

When an atom is in an excited state, after some amount of time, it will decay to a lower energy state emitting a photon in the process. This is known as spontaneous emission. It is one of the three elementary light-matter interactions. If it has not decayed at time t , then the probability that it does so in the next infinitesimal time step $[t, t+\delta t]$, is t -independent. So there is no preferred time at which to decay—in this sense it is a random process. Here we show, by carefully engineering this light-matter interaction, that we can associate it with a clock, where the matter constitutes the clockwork and the spontaneous emission constitutes the ticking of the clock. In particular, we show how to realise the quasi-ideal clock. Said clock has been proven—in an abstract and theoretic sense—to be the most accurate clock permissible by quantum theory, with a polynomial enhancement in precision over the best stochastic clock of the same size. Our results thus demonstrate that the seemingly random process of spontaneous emission can in actual fact, under the right circumstances, be the most regular one permissible by quantum theory. To achieve this we use geometric features and flux-loop insertions to induce symmetry and Berry phases into the light-matter coupling. We also study the entropy the clock produces per tick and show that it also possesses a quantum advantage over that generated from the previously known semi-classical clocks in the literature.

I. INTRODUCTION

Spontaneous emission is the process in which an excited state of matter decays to a lower energy state via the spontaneous emission of a photon. It is the elementary process underlying many light-matter phenomena including luminescence, fluorescence, phosphorescence and is a fundamental component to many technologies such as the laser. The textbook definition tells us that it is a very random process. Indeed, the probability $P(t)$ of the excited state decaying in a time interval $[t, t+\delta t]$ is governed by the same equation as that of radioactive decay:

$$P(t) = \Gamma_0 e^{-t\Gamma_0} \delta t, \quad \Gamma_0 > 0. \quad (1)$$

Yet it is a distinctly quantum-mechanical phenomenon since it cannot be described via classical electromagnetism. Note that this is the most random of all possible processes—given that it has not decayed at time t the probability of decaying in the next infinitesimal time step δt is t -independent. If we were to associate the spontaneous emission process with the tick of a clock, then it would be the worst clock imaginable—bar a clock which doesn't tick at all. Tantamount to this, spontaneous emission is even used for random number generation [1].

Why is standard spontaneous emission so random? The usual situation is when the excited state of matter is an energy-eigenstate. Since such states do not

change over time, they cannot provide any timing information. Therefore, the probability of decaying in an interval $[t, t+\delta t]$ cannot depend on the time t itself. The only consistent distribution with this property is eq. (1). While this description is classical the decay process itself requires one to take into account quantized vacuum fluctuations of the electromagnetic field—indeed, a purely classical description would predict no decay at all. One can characterise the precision of this decay by the ratio $R = \mu^2/\sigma^2$ of the mean over the standard deviation of the time when the spontaneous decay occurred. From eq. (1) it follows an R -value of unity. At the other extreme, a value $R = \infty$ corresponds to a completely deterministic decay time. Thus if we were to use the decay even as the ticking of a clock, $R = \infty$ corresponds to a hypothetical idealised clock.

If one aims to use spontaneous decay for tick of a clock one may try to increase its precision by considering an excited state of matter which is in a superposition of two non-degenerate energy eigenstates, since such states do evolve in time. For concreteness, suppose these two levels form the upper-most two of three equidistant energy levels. Due to the electromagnetic field, this excited state will decay to the ground state at some point in time. One can derive a master equation to describe the three-level system. In doing so, one finds that the quantised electromagnetic field decoheres the superposition and the decay probability is described by a probabilistic mixture over decaying from either the top level to the ground state, or the intermediate level to the ground state. Each of the two decay processes is described by eq. (1). In general by considering general stochastic processes like this one, the

* mischa.woods@gmail.com

best possible achievable R -value can be increased to d , where d is the number of excited states, [2]. By considering generic quantum systems, the in-principle theoretic maximum for a d -dimensional quantum system is an R -value proportional to d^2 in the large-system limit [2].

This latter remark follows from putting two observations together: the process of spontaneous emission and the nascent field of quantum clocks both have in common that they are described mathematically via quantum dynamical semi-groups. Indeed, recently an abstract theoretical quantum clock was proposed which demonstrably achieved a quantum advantage [2]. It was later shown that this clock achieved the theoretical maximum accuracy allowed by quantum mechanics [3]. However, the proof is abstract and information-theoretic with no clear system in which it can be realised. Here, we prove that the seemingly random process of spontaneous decay, can in actual fact represent the most precise process permissible by quantum mechanics within the framework of Markovian processes, thus even surpassing the classical limit. Spontaneous emission is already an important process in many technologies, but was never considered useful for producing well-timed emitted photons. Our work suggests that spontaneous emission could be useful as a quantum technology producing extremely precise time-delayed photons and de-excitations of matter.

This manuscript. In a nutshell, we take advantage of two quantum phenomena to achieve a spontaneously emitted photon which is at the quantum limit of precision—an R -value of d^2 . First, we show that if the energy levels over which the excited state of matter is initialised to are very close together in comparison with the lower energy states it can decay to, it will maintain quantum decoherence despite the presence of the electromagnetic field. This however is not sufficient to achieve the fundamental limit of precision. Secondly, we show that if the dipole moments connecting the excited states with the ground states satisfy a certain symmetry—which can be induced by a geometrical Berry phase—then the decay channels are the discrete Fourier transform modes of the excited energy levels. These modes have support on all the excited energy levels and as such, the detection of the matter in a ground state due to it spontaneously decaying provides little information about the excited energy level(s) it came from. It turns out that this uncertainty in energy permits the uncertainty in the decay time to be extremely small.

Paper outline. In section II we review the abstract clock model of which the quasi-ideal clock is a special case and plot its accuracy in low dimensions using new techniques developed here. With this in mind, we derive from first principles the quasi-ideal clock in the context of spontaneous emission in section III. Given a model stemming from a physical environment, we are in the position to faithfully calculate the entropy produced per tick of our clock; we do so in section IV. We end with a discussion and conclusion in section V.

II. GENERIC CLOCK MODEL, THE QUASI-IDEAL CLOCK AND PRECISION

We start by reviewing the generic clock model and a particular abstract quantum clock called the quasi-ideal clock [2, 4] which achieves the maximum precision out of all the clocks in the model. We finish by numerically optimising precision over the parameters of the model in low dimensions to show that the optimal quadratic scaling is still achievable in low dimensions. This section is important because in section III the quasi-ideal clock is realised via a light-matter interaction and hence the claim that it is the most accurate clock is to be understood in this context.

The clock model consists in a clockwork state and a register state. The aim of the clockwork is to capture the timing resources while the register (or “clock face”) records the time. Since we aim to emit classical information about time, the register will be classical, i.e. the emission of a “tick” is the process in which the register changes from one orthonormal state to the next—analogously to the changes in the second hand on a wall clock. The clockwork on the other hand, can change continuously and in principle evolve to any quantum state. We denote its initial state by ρ_{CR}^0 .

The principle aim of our clock model is to capture the resources needed to run a clock which produces timing at a certain precision. We therefore should put some constraints on the dynamical channel $\mathcal{M}_{\text{CR} \rightarrow \text{CR}}^t$ responsible for evolving the clock forward according to background time t . Arguably the most basic of such constraints is that the channel is divisible:

$$\mathcal{M}_{\text{CR} \rightarrow \text{CR}}^{t_1+t_2}(\rho_{\text{CR}}) = \mathcal{M}_{\text{CR} \rightarrow \text{CR}}^{t_1} \circ \mathcal{M}_{\text{CR} \rightarrow \text{CR}}^{t_2}(\rho_{\text{CR}}) \quad (2)$$

for any two times $t_1, t_2 \geq 0$ and clockwork-register state ρ_{CR} . Otherwise, there is the possibility that an unaccounted-for timing resource in the environment is providing timing information, e.g. another clock of unforgotten resource requirements. One can impose a few more conditions, namely that the clock should not skip a tick and its precision should not depend on the initial position of the register [4]. Equation (2) and these additional two other conditions are satisfied if and only if $\mathcal{M}_{\text{CR} \rightarrow \text{CR}}^t$ is of the form

$$\mathcal{M}_{\text{CR} \rightarrow \text{CR}}^t = e^{t\mathcal{L}_{\text{CR}}}, \quad (3)$$

for

$$\begin{aligned} \mathcal{L}_{\text{CR}}(\cdot) = & -i[\tilde{H}, (\cdot)] + \sum_{j=1}^{N_T} \tilde{L}_j(\cdot)\tilde{L}_j^\dagger - \frac{1}{2} \left\{ \tilde{L}_j^\dagger \tilde{L}_j, (\cdot) \right\} \\ & + \sum_{j=1}^{N_T} \underbrace{\tilde{J}_j(\cdot)\tilde{J}_j^\dagger}_{\text{tick generator}} - \frac{1}{2} \left\{ \tilde{J}_j^\dagger \tilde{J}_j, (\cdot) \right\}. \end{aligned} \quad (4)$$

Here $\tilde{H} = H_{\text{C}} \otimes \mathbb{1}_{\text{R}}$, $\tilde{L}_j = L_j \otimes \mathbb{1}_{\text{R}}$, $\tilde{J}_j = J_j \otimes O_{\text{R}}$ and $O_{\text{R}} := |1\rangle\langle 0|_{\text{R}} + |2\rangle\langle 1|_{\text{R}} + |3\rangle\langle 2|_{\text{R}} + \dots + |N_T\rangle\langle N_T - 1|_{\text{R}}$,

where $N_T \in \mathbb{N}$ and $N_T + 1$ is the dimension of the register. Further, H_C is hermitian, whereas $\{J_j\}_j$, $\{L_j\}_j$ are linear.

The ticks are generated by the term marked as *tick generator*, the other $\{\tilde{J}_j\}_j$ terms generate a type of back-reaction on the clockwork as a consequence of ticking. The $\{L_j\}_j$ terms are environmental noise not necessarily related to the ticking process itself. Initiating the clock state to one where it has not yet ticked, $\rho_{\text{CR}} = \rho_C \otimes |0\rangle\langle 0|_{\text{R}}$, the probability density to observe the register in the state $|1\rangle\langle 1|_{\text{R}}$ is given by

$$P_{\text{tick}}(t) = \text{tr} \left(\sum_{j=1}^{N_T} J_j(\rho_{\text{C}}^{\text{nt}}(t)) J_j^\dagger \right), \quad (5)$$

where $\rho_{\text{C}}^{\text{nt}}(t) := e^{t\mathcal{L}_{\text{C}}^{\text{nt}}} \rho_{\text{C}}^0 / \text{tr} \left[e^{t\mathcal{L}_{\text{C}}^{\text{nt}}} \rho_{\text{C}}^0 \right]$ is the time-evolved initial clockwork state conditioned on not having observed a tick at time t , and where $\mathcal{L}_{\text{C}}^{\text{nt}}(\cdot) := \text{tr}_{\text{R}}[\mathcal{L}_{\text{CR}}(\cdot) \otimes |0\rangle\langle 0|_{\text{R}}] |0\rangle\langle 0|_{\text{R}}$, as per [4]. Equation (5) is the *delay function* (or *waiting time*) of the first tick. Given a particular clock of the form eq. (3), the precision of its first tick is defined by

$$R := \frac{\mu^2}{\sigma^2}, \quad \mu := \int_0^\infty dt P_{\text{tick}}(t) t, \quad \sigma := \int_0^\infty dt P_{\text{tick}}(t) (t - \mu)^2. \quad (6)$$

Since the register is a classical counter it can be omitted from the dynamical semigroup description while still reproducing the correct dynamics for the clockwork. In this case the probability of ticking corresponds to the probability of observing exactly one jump and mathematically corresponds to tracing out the register [4]. The resulting clockwork dynamics corresponds to the replacements $\tilde{H} \rightarrow H_C$, $\{\tilde{L}_j \rightarrow L_j\}$, $\{\tilde{J}_j \rightarrow J_j\}$ in eq. (4). In section III the presence of a photo/charge detector is continuously measuring the electromagnetic environment and the detection of a photon or corresponding change in charge represents the classical register.

Any clock in the model can be specified by providing the initial clockwork state, and matrices H_C , $\{J_j\}_j$, $\{L_j\}_j$. Quasi-ideal clocks [2, 4, 5] are defined by

$$H_C = \sum_{n=0}^{d-1} \omega_0 n |E_n\rangle\langle E_n|, \quad (7)$$

$$\{L_j = 0, J_j = \sqrt{2V_j} |\psi_{\text{C}}\rangle\langle t_j| \}_{j=0}^{d-1}, \quad (8)$$

where $|\psi_{\text{C}}\rangle$ is the initial clockwork state, $\rho_{\text{C}}^0 = |\psi_{\text{C}}\rangle\langle\psi_{\text{C}}|$. The coefficients $V_j \geq 0$ are coupling coefficients to be defined. The states

$$|t_k\rangle = \frac{1}{\sqrt{d}} \sum_{j=0}^{d-1} e^{-i2\pi j k/d} |E_j\rangle \quad (9)$$

correspond to the discrete Fourier transform of the energy basis. This model is parametrized by the choice of

$|\psi_{\text{C}}\rangle$ and $\{V_j\}_j$. It was proven in [2] that this clock can achieve a precision of the m^{th} tick of

$$R(d) \propto md^2 \text{ as } d \rightarrow \infty \quad (10)$$

for an appropriately chosen set $\{V_j\}_j$ parametrized by d and quasi-ideal initial state $|\psi_{\text{C}}\rangle$. It was also shown that the mean ticking time μ can take on any value—although in practice may be limited if the strength of the interactions is bounded [6]. It was proven in [3] that all clocks satisfying the axioms of [4] have a precision which is upper bounded by a quadratic function of the dimension, thus proving the optimality of the quasi-ideal clock. Whether this quadratic scaling of the precision could be achieved in low dimensions remained an open question. The answer is of particular interest in the current context since initial experimental realisations are likely to be more feasible in low dimensions. In fig. 1 we show via a numerical optimization method developed in appendix E, that it can. Finally, no experiment will be perfectly accurate, we thus check that the quantum advantage is indeed robust to noise. In fig. 2 we plot the decrease in accuracy for the optimal case when allowing for a small variation in the coupling coefficients and initial state. Since this is the worst-case scenario, experiments with said errors are likely to represent clocks of higher precision.

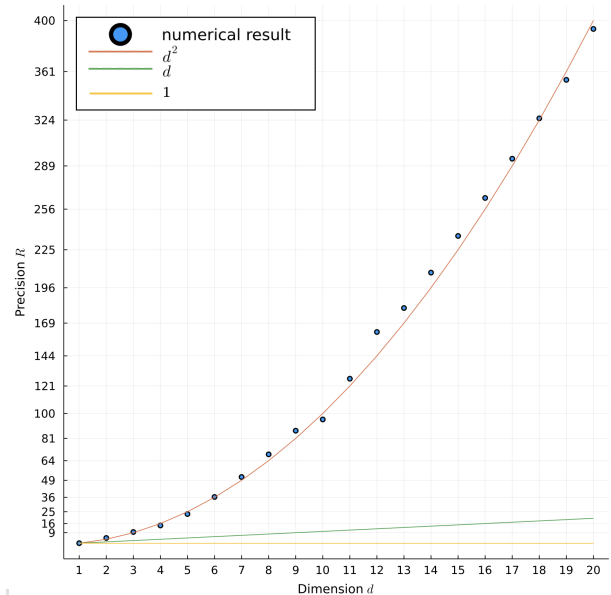


FIG. 1. The plot shows the numerically optimized precision (blue dots) in low dimensions $d \leq 20$. We observe a d^2 scaling (orange line) of the precision, demonstrating the quantum advantage. The optimal stochastic precision is also illustrated (green line), as well as the precision of conventional spontaneous emission, $R = 1$; (yellow line). Observe that in certain dimensions the numerically optimized precision can be higher than d^2 while in others it is slightly below.

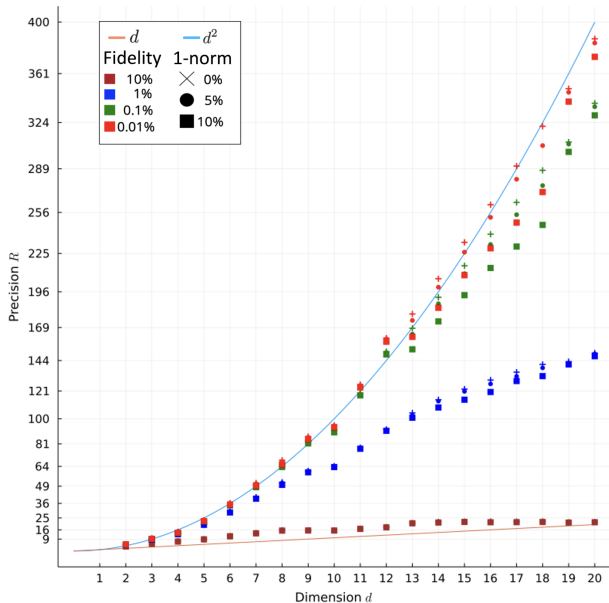


FIG. 2. The plot shows worst-case-scenario robustness of the precision subject to an initial-state-preparation constraint and a constraint on the channel generating the dynamics. In particular, the worst-case-scenario robustness of the precision is achieved by minimizing R over all initial clockwork states of a fixed fidelity away from the optimal initial clockwork state, and minimizing R over coupling coefficients $\{V_j\}_j$ subject to a fixed value of the 1-norm of the difference in coupling coefficients $\{V_j\}_j$ relative to their optimal values. Data is represented as a percentage change in fidelity and 1-norm from their optimal values. Observe that the clock’s precision only becomes comparable with the optimal classical clock when there is a 10% error in both fidelity and 1-norm collectively. This demonstrates that the quantum advantage is quite robust against errors.

III. MACROSCOPIC DERIVATION VIA LIGHT-MATTER INTERACTIONS

We are now in the position to provide a macroscopic setup which gives rise to a light-matter realisation of the quasi-ideal clock. For this, we need to find an environment, an initial state on it, and a Hamiltonian over the clockwork, register and environment such that when we trace out the environment, we achieve the same dynamics as that generated by the quasi-ideal clock dynamical semigroup.

We consider an electromagnetic environment and the clockwork will consist in the wave function of a negatively charged particle whose initial clockwork state is on a ring called primary ring and centred at the origin of the x - y plane. At a distance $|z_0|$ along the z -axis below the plane lays a secondary ring of positive charge q . The charge difference and separation mean that the secondary ring is of lower energy and the pair form an electric dipole, with dipole vector $\vec{r} = (0, 0, z_0)$. The clockwork state can decay from the primary ring to the secondary ring via spontaneous photon emission into

the electromagnetic field environment—this is the mechanism with which ticks will occur. Later we will allow for more decay channels by adding more secondary rings at different heights along the z -axis.

A. The Hamiltonian part

Here we discuss how to construct the Hamiltonian part of the Lindbladian.

The primary ring is centred at $z = 0$ along the z -axis and has d equally spaced (in the ϑ angle) identical wells. Therefore, the primary ring has a d -fold degenerate ground state. The j^{th} degenerate ground state corresponds to the energy level $|E_j\rangle$. We will later show how to lift the degeneracy to achieve the truncated harmonic spectrum of eq. (7). The secondary ring has m flux loops inserted, leading to a ground state on the secondary ring given by

$$|2^{\text{ndry}}, m\rangle := \int_0^\infty dr r \int_{-\infty}^\infty dz \int_0^{2\pi} d\vartheta f(r, z) \frac{e^{im\vartheta}}{\sqrt{2\pi R}} |r\rangle|z\rangle|\vartheta\rangle, \quad (11)$$

where r, z, ϑ are cylindrical-polar coordinates, R is the radius of the ring, $f(r, z)$ is an arbitrary normalised wave function over r and z . The mean separation between primary and secondary rings controls the interaction strength between them. Meanwhile, m denotes the number of flux quanta giving rise to the Berry phase $e^{im\vartheta}$. Thus the change of flux quanta allows for control of the matrix elements involving this ground state—we will see how to choose m later. See Fig. 3 for a depiction of this setup.

The secondary ring serves as a decay channel for the d -dimensional Hilbert space of the primary ring. We can demand that it serves as an energetically well-separated ground state by virtue of the positive particle. Therefore, every state of the primary ring can decay. Under these conditions the coupling between the levels of the primary ring $\{|E_j\rangle\}_{j=0}^{d-1}$ and the secondary ring are given by the dipole. We will see how the dipole matrix elements enter the dissipater later, but for now let us note some important geometry-induced symmetries. The wave functions $\psi_j(z, r, \vartheta)$ corresponding to the states $\{|E_j\rangle\}_{j=0}^{d-1}$ satisfy $\psi_j(z, r, \vartheta) = \psi_0(z, r, \vartheta + 2\pi j/d)$ due to the rotational symmetry. Therefore, the $s \in \{r, z, \vartheta\}$ component of the dipole matrix element connecting $|E_j\rangle$ with $|2^{\text{ndry}}, m\rangle$ is

$$[D_s]_{m,j} := q \langle 2^{\text{ndry}}, m | \hat{s} | E_j \rangle = e^{-i2\pi j m/d} [D_s]_{m,0}, \quad (12)$$

where we have taken into account the orthogonality of $\{|E_j\rangle\}_j$ and $|2^{\text{ndry}}, m\rangle$. Note how the phase factor in eq. (12) is identical to the ones appearing in eq. (9) when the number of inserted flux loops m is equal to k . This is a key observation which has resulted from the geometry of the rings and Berry phase, and will turn out to be critical for achieving the quantum advantage in time

keeping. It is important that there are no spontaneous transitions between states we do not want to associate with the clock ticking. Therefore, transitions between such states should be dipole forbidden. This is the case here, since the wave functions of $\{|E_j\rangle\}_j$ have approximately zero overlap due to the spacing between the wells resulting in a zero dipole matrix elements between any pair $|E_j\rangle, |E_l\rangle$.

We can also add additional copies of the secondary ring above and below the primary ring in the x - y plane all centred along the z -axis and parallel to one another. These additional secondary rings are useful when each one of them has a different number m of flux loops inserted. Each additional secondary ring allows for a new decay channel from the primary ring whose strength and energy can be tuned by adjusting its separation along the z -axis from the primary ring centred at $z = 0$. With two secondary rings, we can place them on opposite sides of the primary ring since its only the absolute value of the separations which matter—not the sign. With three or more rings, with the current geometry, this will always lead to two or more rings being closer along the z -axis to each other than to the primary ring. While within the dipole approximation this is perfectly sound, in reality, this relatively small inter-secondary-ring separation may lead to virtual transitions between the rings. Luckily, as we will see in section III B the ultimate precision limit can already be achieved with just two rings—at least up to moderately large dimensions. For completeness, we assume a total of $L \leq d$ secondary rings with $m_1, \dots, m_L \in \{0, 1, \dots, d-1\}$ flux loops respectively. Therefore, the total free Hamiltonian of the clockwork is thus

$$H_S = H_C - \sum_{j=0}^{L-1} \omega_{0m_j} |2^{\text{ndry}}, m_j\rangle \langle 2^{\text{ndry}}, m_j|, \quad (13)$$

where $\omega_{0m_j} > 0$ is the energy gap between the $|E_0\rangle$ eigenstate of H_C and the j^{th} secondary ring. The minus sign in eq. (13) is due to the energy levels of the secondary rings lying below that of H_C .

Thus far, the primary ring is energetically degenerate, and so there is no free dynamics. We now add a potential to the lower ring to lift said degeneracy and achieve the harmonic spectrum of H_C . Taking inspiration from tight-binding models (see, e.g. [7]), we show that such a potential is always achievable; we leave the details for appendix B. While it creates a significant difference in the free dynamics of the clockwork, its effect on the dipole moment relations eq. (11) is neglectable. This is important since such relationships are crucial for our clock to work. We calculate the dipole moments numerically to verify that eq. (11) can indeed be satisfied to arbitrary precision. We take into account that the states $\{|E_j\rangle\}_j$ are only approximately orthogonal due to the small overlap in the ground state wave functions of the potential wells of the primary ring.

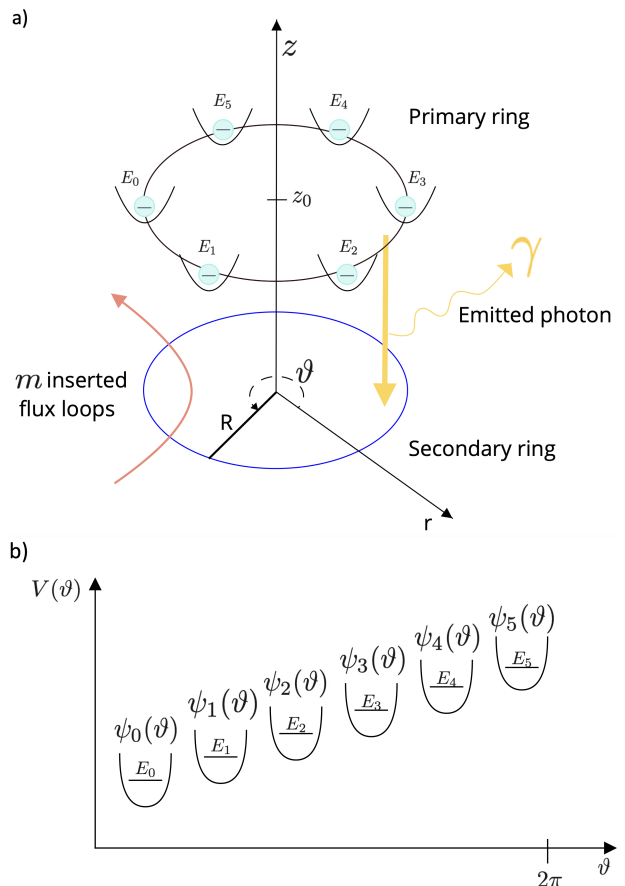


FIG. 3. Depiction of the setup in $d = 6$. **a)**: an excited electron is in a judiciously chosen superposition state with support over the ground states of 6 degenerate oscillators. The former are equally-distantly placed around a ring—the so-called primary ring. At lower energy and a distance z_0 below it, lays another ring—the secondary ring—threaded with m flux loops. The primary and secondary rings interact via the background quantised electromagnetic field. This permits the electron to spontaneously decay to the secondary-ring state. **b)**: depiction of the primary ring when an additional potential has been activated to lift its degeneracy.

B. The Dissipator part

Here we discuss how to derive the dissipator part of the Lindbladian. For simplicity, we will consider only one secondary ring with m flux loops and frequency ω_{0m} . We explain how the result generalises to the multi-secondary-ring case at the end.

The bath of the system is the Fock space of the electromagnetic field which interacts with the negatively charged particle (clockwork state) through spontaneous emission of a photon. To achieve this, we assume that the initial state of the electromagnetic field is a low-temperature bath (an infinite-dimensional Gibbs state). The low temperature is important, since it implies that the mean photon number in the environment is tiny on

average, and thus the probability of spontaneous absorption is neglectable as we will see.

Secondly, the typical correlation times of the photons are much shorter than the typical timescale of the matter interactions. Thus light-matter interactions can be effectively modelled with a Markovian evolution. This is known as the Born-Markov approximation.

As is standard in light-matter interactions, we will work in the dipole approximation so that the interaction Hamiltonian of Fock space and system is given by $H_I = \vec{D} \cdot \vec{E} = D_z \otimes E_z$, where \vec{D} , \vec{E} are the dipole and electric field operators, and as we have seen the dipole moment for the matter is aligned along the z -axis. Next, applying the Born-Markov approximation we arrive at the standard textbook result for the system state $\rho_S(t)$ in the interaction picture

$$\begin{aligned} \frac{d}{dt} \rho_S^I(t) = & \sum_{\omega, \omega'} e^{i(\omega' - \omega)t} \Gamma(\omega) \left(D_z(\omega) \rho_S^I(t) D_z^\dagger(\omega') \right. \\ & \left. - D_z^\dagger(\omega') D_z(\omega) \rho_S^I(t) \right) + \text{h.c.}, \end{aligned} \quad (14)$$

where $\Gamma(\omega)$ encodes the bath correlations and we have expanded the dipole moments into terms of equal energy spacing:

$$D_z(\omega) := \sum_{\varepsilon' = \varepsilon = \omega} \Pi(\varepsilon) D_z \Pi(\varepsilon'), \quad (15)$$

with $\Pi(\varepsilon)$, $\Pi(\varepsilon')$ projectors onto subspaces of energy ε and ε' , respectively of the free clockwork Hamiltonian, eq. (13).

Typically, at this point, one invokes the secular approximation also known as rotating-wave approximation (RWA): $e^{i(\omega' - \omega)t} \approx \delta(\omega - \omega')$. The approximation corresponds to widely separated transitions, so that one can resolve from which energy level the decay occurred. This approximation does not hold in our case for all frequencies, as a good clock only has a single fast oscillation corresponding to a tick, because $\omega_{0m} \gg (d-1)\omega_0$. Therefore, we should not observe multiple oscillations of the clockwork before a tick occurs and averaging of phases does not hold for the frequency range $-(d-1)\omega_0 \leq \omega' - \omega \leq (d-1)\omega_0$ appearing in eq. (14). Consequently, we work in a limit where the transitions between energy levels of the truncated oscillator Hamiltonian H_C cannot be cleanly resolved. On an intuitive level, the advantage of doing so can be understood in terms of the time-energy uncertainty relation: this large uncertainty in energy allows for high certainty in time. Lastly, the aforementioned zero dipole elements of the inter-primary-ring transitions also play a crucial role: they block any remaining decay channels other than the decay channel to the secondary ring.

Now let us turn to the bath correlations. As is customary, we will neglect the imaginary part as it only leads to a small type of lamb shift in the energy levels. To calculate the real part, we note that we are assuming that the

quantised electromagnetic field is isotropic. This leads to the classic result

$$\Gamma(\omega) = \frac{2\omega^3}{3c^3} (1 + N(\omega)). \quad (16)$$

When $\omega > 0$, $N(\omega)$ is the number of photons with frequency ω in the Fock space and given by the Planck distribution. The terms give rise to photo emission and the clock ticking. It is via $N(\omega)$ that the temperature of the electromagnetic field enters our model. The $\omega < 0$ case correspond to the reverse process and is related to the aforementioned process via $N(\omega) = -(1 + N(-\omega))$. In our low-temperature limit $N(\omega) \approx 0$, and

$$\Gamma(\omega) = \frac{2\omega^3}{3c^3}, \quad \Gamma(-\omega) = 0 \quad (17)$$

for $\omega \geq 0$. We numerically show the robustness of this approximation for experimentally-feasible low temperatures in fig. 4 and provide the full derivation in appendix A. Note that at higher temperatures such as room temperature, the spontaneous emission process would still occur—just that this process would no longer be isolated as spontaneous absorption would also be present.

We can now return to the dipole transition elements. The only relevant terms are $\langle 2^{\text{ndry}}, m | D_z(\omega_{0m} + n\omega_0) | E_n \rangle$ for $n = 0, 1, \dots, d-1$ since the other terms are either zero or irrelevant due to $\Gamma(\omega)$ being zero. Moreover, due to geometry and the Berry phase, these dipole elements are identical up to a well-defined time independent phase as seen in eq. (12). Putting everything together and going back to the Schrödinger picture, we arrive at

$$\frac{d}{dt} \rho_S(t) = \hat{J}_m \rho_S(t) \hat{J}_m^\dagger - \frac{1}{2} \left\{ \hat{J}_m^\dagger \hat{J}_m, \rho_S(t) \right\}, \quad (18)$$

where $\hat{J}_m := \sqrt{2d\Gamma(\omega_{0m})} | \langle 2^{\text{ndry}}, m | D_z(\omega_{0m}) | E_0 \rangle | | 2^{\text{ndry}}, m \rangle \langle t_m |$. In the case of additional secondary rings with inserted fluxes $m = 0, 1, \dots, d-1$, we would sum over m from zero to $d-1$. Now suppose we choose $d\Gamma(\omega_{0m}) | \langle 2^{\text{ndry}}, m | D_z(\omega_{0m}) | E_0 \rangle |$ equal to V_m in eq. (8). We can do this, for example, by varying the separation of the secondary rings to the primary one. We have now achieved an implementation of the quasi-ideal clock up to the fact that now, after a tick, the clockwork is set to state $| 2^{\text{ndry}}, m \rangle$ rather than the initial state $| \psi_C \rangle$ on the primary ring. The classical tick register can either be implemented by detecting the change in charge of the secondary ring to which the negatively charged particle jumped to or by detecting the emitted photon itself. But how many secondary rings to we actually need to achieve the optimal precision? As discussed in section III A, there would be additional hurdles to overcome going beyond two secondary rings due to the possibility of virtual inter-secondary-ring transitions arising. In fig. 5 we numerically optimise the precision when only allowing for one and two secondary rings. Importantly, we observe, at least up to moderately large dimensions,

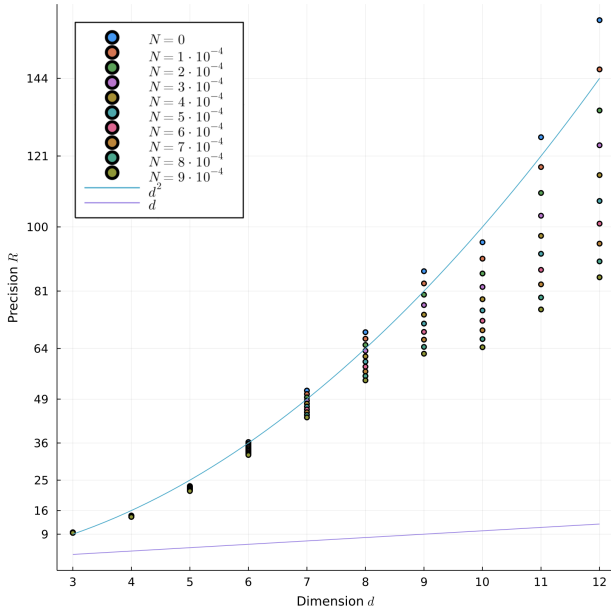


FIG. 4. Precision as a function of mean bath photon occupancy number $N(\omega_{0m})$ for the optimal clock. The $N = 0$ case is the same as in fig. 1. (Plots d and d^2 are guides to the eye). If $N(\omega_{0m}) \approx 0$ is violated, we have a certain probability for the time reverse process by photon absorption. As we consider a thermal state, it obeys Bose-Einstein statistics. At optical frequencies at room temperature one can easily achieve $N(\omega_{0m}) \approx 10^{-50}$ which from the plot we see is effectively zero. At microwave frequencies we have higher numbers. Luckily, cooling has an exponential effect on the occupation number, meaning that reducing the temperature by a half reduces $N(\omega_{0m})$ by one order of magnitude. Concretely, operating at $1meV$, at $T = 10mK$, we have $N(\omega_{0m}) \approx 10^{-5}$. While this error is appreciable in the plot, it is still very small relative to the classical bound $R = d$.

that just two rings suffice to effectively achieve maximal accuracy. It is unknown whether more decay channels are needed in higher dimensions to achieve the optimal precision. We discuss how this model can be generalised to a multi-consecutive-tick setting in appendix C.

IV. ENTROPY PRODUCTION PER TICK

In this section we examine the entropy generated per tick and its relation to accuracy and clockwork dimension.

The entropy production per tick is defined as the average entropy flux out of the clockwork between two ticks. It corresponds to the amount of entropy flowing into an open quantum system from its environment. For a generic dynamical semi-group with Lindblad operator $\mathcal{L}(\cdot) = [H_S, (\cdot)] + \mathcal{D}(\cdot)$ where \mathcal{D} is the dissipative part, the entropy flux produced during an infinitesimal time step

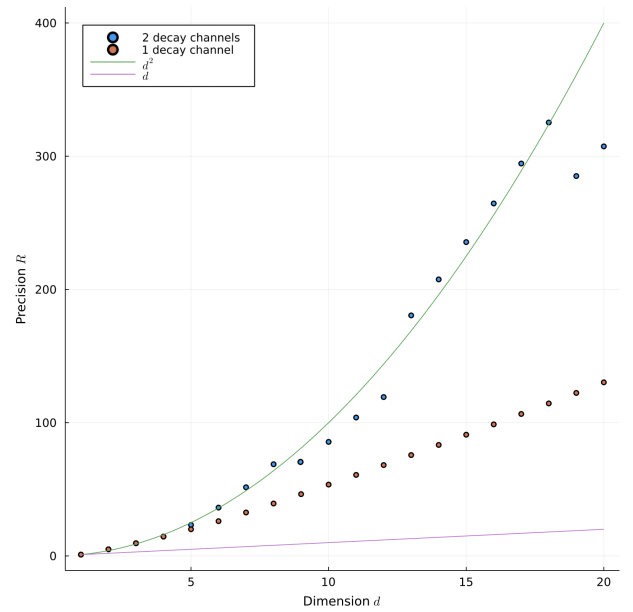


FIG. 5. Numerically optimised precision in low dimensions when restricting to one and two decay channels. We observe that one decay channel illustrates linear scaling which is better than the optimal stochastic case but significantly worse than the optimal quantum case when all decay channels are available (recall fig. 1). However, when two decay channels are available, we are close to achieving the (optimal) scaling corresponding to when all d decay channels are available; at least for dimension $d \leq 20$. What is more, this scaling is achieved for decay Fourier modes corresponding to the least number of flux loops: modes $|t_0\rangle$, $|t_1\rangle$ and $m_1 = 0$, $m_2 = 2$ respectively. Notice now the precision for $d = 19$ and $d = 20$ are less than for $d = 18$ in the 2-decay-channel case. This demonstrates that when restricting the number of decay channels, higher-dimensional decay channels do not necessarily increase the accuracy. This is consistent since $\{|t_k\rangle\}_k$ is not a subset of $\{|t_l\rangle\}_l$ for $k < l$.

dt for an initial state $\rho_S(t)$ is

$$dJ(t) := -\beta \operatorname{tr}[H_S \mathcal{D}(\rho_S(t))] dt = \operatorname{tr} \left[\mathcal{L}(\rho_S(t)) \ln(\rho_S^\beta) \right] dt, \quad (19)$$

where ρ_S^β is the system's Gibbs state, $\rho_S^\beta := e^{-\beta H_S} / Z_\beta$ at the ambient temperature β^{-1} [8, 9].

It is well-known that entropy is an observer-dependent quantity since different observers may have different information. In the case of a clock, we have to adjust this definition to take into account that the ticks are classical and readily accessible information. Let us define the entropy for the k^{th} tick as follows: We start with the state of the clockwork just after ticking $k - 1$ times (or the initial clockwork state ρ_C^0 in the case of $k = 1$). We then integrate the infinitesimal quantity eq. (19) while conditioning on not ticking up to time t followed by multiplying by the probability that the k^{th} tick occurs at

time t . Finally, since t is unknown¹, we integrate over all $t \geq 0$. In the case of a reset clock, the quantity is the same for all ticks and is given by

$$\Delta S_{\text{tick}} := \int_0^\infty dt P_{\text{tick}}(t) \int_0^t ds \text{tr} \left[\mathcal{L}_C^{\text{nt}}(\rho_C^{\text{nt}}(s)) \ln(\rho_C^\beta) \right], \quad (20)$$

where $\mathcal{L}_C^{\text{nt}}$ and $\rho_C^{\text{nt}}(t)$ are the clockwork Lindbladian and state respectively conditioned on having not observed a tick as per eq. (5). Other related notions of clock entropy production can be found in [10].

A clock based on thermodynamic absorption principles was introduced in [11]. This thermal absorption clock has a clockwork consisting in a ladder Hamiltonian with equidistant spacing and dimension d .² The population starts at the bottom of the ladder and is driven upwards by work performed on it by the flow of heat from a hot thermal bath to a cold thermal bath at inverse temperatures β_h, β_c respectively. The ladder does not couple directly to the thermal baths, but instead couples to two qubits (of energy gaps E_c and E_h) which are maintained at thermal equilibrium with the hot and cold baths respectively. The three-body interaction between the hot and cold qubits and the ladder induces an effective two-body coupling between a virtual qubit with inverted population and every step of the ladder. The population of the ladder then equilibrates with the virtual bath. Since the virtual qubit has population inversion this equilibration causes the population of the ladder to be driven up it. The amount of heat dissipated to the cold bath every time the population climbs one run of the ladder is $E_w = (E_h - E_c)$. When the population reaches the top of the ladder a tick occurs via the emission of a photon. This allows for the population to be re-set to its initial state at the bottom of the ladder and the process to start over again. In this special case, it is readily clear how much entropy is produced per tick—the amount of entropy produced for the population to climb the ladder. We compare this quantity to that generated by our definition in fig. 8. We find that the definitions agree and more generally that the entropy produced per tick is approximately given by

$$\Delta S_{\text{tick}} \approx \beta_v(Q_h - Q_c) = \beta_h Q_h - \beta_c Q_c \quad (21)$$

$$= (\beta_c - \beta_h)Q_c - \beta_h E_\gamma, \quad (22)$$

where β_v is the inverse temperature of the virtual thermal bath, $Q_h := (d-1)E_h$, is the total heat flowing into the ladder and $Q_c := (d-1)E_c$ the total amount flowing out

of it during the process in which the population reaches the top of the ladder where the tick occurs. The second line follows from defining $E_\gamma := (d-1)\omega$ and puts into focus the fact that the entropy per tick has two contributions: an entropy sink (the cold bath) and the entropy associated with emission of the photon at energy E_γ . The latter is in principle recoverable and could be recycled as heat back into the hot bath. However, since the aim is to derive fundamental lower bounds, it can be kept without issue. The right hand side of eq. (21) is manifestly proportional to the dimension. However, this relationship only holds approximately when Q_c/E_w is much less than the dimension. Otherwise non-linearities due to reflections from ladder boundaries become relevant. The exact dependency is plotted in fig. 7. In [11] the precision R of each tick was also found to be approximately proportional to the ladder dimension d . One can write the precision per tick as a function of the minimum entropy per tick by eliminating the explicit d dependency. In the large d limit the boundary effects vanish and one finds that a minimal entropy per tick for this model is [11]

$$R = \frac{\Delta S_{\text{tick}}}{2}. \quad (23)$$

It was reasoned that while this linear scaling was derived for a specific model, that it should in fact be a fundamental lower bound on the amount of entropy required to produce a tick of the stated precision. However, said reasoning was classical in nature and did not take into account quantum effects. Nevertheless, the paper is commonly cited in the literature as providing a fundamental limit on the entropy produced per tick.

Let us now examine the entropy per tick as a function of the clockwork dimension for the light-matter quasi-ideal clock. From the numerics in fig. 6 we also observe a linear relationship between the clockwork dimension d and the entropy per tick, namely

$$\Delta S_{\text{tick}} \approx \beta(\omega_\gamma + \omega_0 d/2), \quad (24)$$

where recall β denotes the inverse temperature of the thermal bath. The linear dependency with β can be understood by observing that at low bath temperatures (large β) the emission of a photon into the bath perturbs it much more than if it were at a high temperature, and creates more entropy in the process. The quantity $\beta\omega_\gamma \in \{\beta\omega_{0m_1}, \beta\omega_{0m_2}, \dots, \beta\omega_{0m_{L-1}}\}$ is just the energy emitted by the photon producing the tick, while $\omega_0 d/2$ is the mean energy of the initial state of the clockwork. This is essentially the same relationship we observed for the thermal absorption clock [11] in eq. (21) but without the cold bath which acted as an entropy sink. Importantly, in both cases the entropy per tick is directly proportional to the dimension of the clockwork. However, as has been shown, the precision R for the quasi-ideal clock scales quadratically with the dimension d , therefore by substitution we find that the quasi-ideal clock realised via a

¹ We only observe the tick, but not the background time t itself. If the clock is good, they will be correlated but only equal in an idealised clock.

² The total dimension of the clockwork is $4d$, since each of the two baths thermalise a clockwork qubit, which in turn interact with the d -dimensional ladder.

thermal environment yields a *quadratic* relationship between the entropy per tick and precision. Namely

$$R \approx \left(\frac{\Delta S_{\text{tick}}}{\beta} - \omega_\gamma \right)^2 \frac{4}{\omega_0^2} \quad (25)$$

for small β^{-1} . As such, the quasi-ideal clock can produce ticks of higher precision at the same entropy expense, thus demonstrating that eq. (23) is not a lower bound.

As discussed in appendix C, the clockwork is not automatically re-set to its initial value. Since the classical decay channels are physically distinguishable one can in principle tell which of the states $\{|2^{\text{ndry}}, m_j\rangle\}$ the clockwork is in after the tick occurs in an actual experiment. Since the initial state $|\psi_C\rangle$ is also pure, only a (entropy-preserving) unitary transformation is required to re-set the clock. This is in stark contrast to the irreversible process of ticking. As such, the inclusion of the resetting of the clockwork should be realisable without incurring a net entropy flux beyond that associated with applying the unitary transformation. The initial state $|\psi_C\rangle$ is of higher energy and thus the unitary will not be energy preserving. So if the source of energy is not pure, then there will be an entropic cost in using it to reset the clock. However, characterising such costs is a generic question for applying non-energy preserving unitaries and is not related to clocks per se. Moreover, as seen from eq. (24) the entropy per tick scales linearly with d and the initial state $|\psi_C\rangle$ only has support of d energy levels, so even if the entropy required to reset the initial state from any of the secondary-ring states $\{|2^{\text{ndry}}, m_j\rangle\}$, we would still obtain a precision R which scales quadratically with the entropy production as in eq. (25). There is another source of entropy associated with the tick-register itself—it also requires re-setting with the usual Launderer erasure cost associated with it. This is of a different nature and discussed in [10].

V. DISCUSSION AND CONCLUSION

In this manuscript we have considered one of the most elementary processes in light-matter interactions: spontaneous emission. In its standard form the emission time is uniform in the sense that the probability of decaying at any given instant, for which it has not decayed already, is independent of the current time. We have proven that by judiciously selecting the excited state and the light-matter coupling, this process can be tuned so that its decay time is the most regular process permitted by quantum mechanics as a function of available energy and dimension in any Markovian setting.

It had been shown that a clock can be defined axiomatically from basic principles about what a clock should be [4], and that the abstract and theoretic quasi-ideal clock is asymptotically the most precise clock permissible [2]. By identifying the matter emitter with the clockwork of a clock, and the spontaneously emitted photon with the

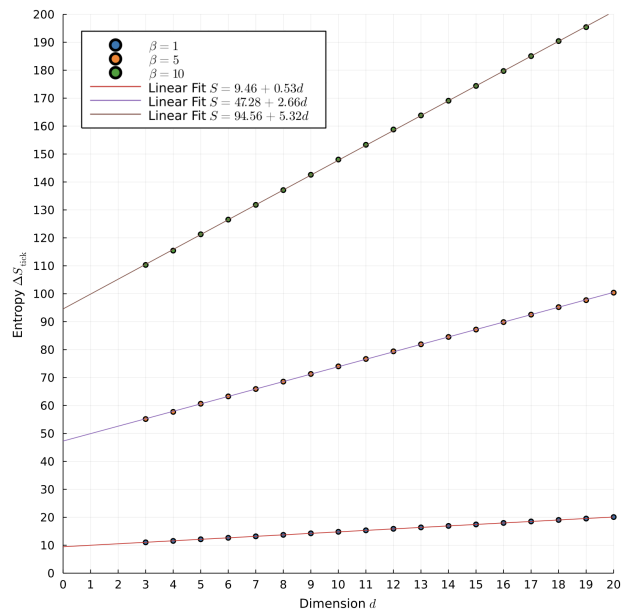


FIG. 6. Entropy per tick for the light-matter implementation for the optimal quasi-ideal clock for different inverse bath temperatures β^{-1} .

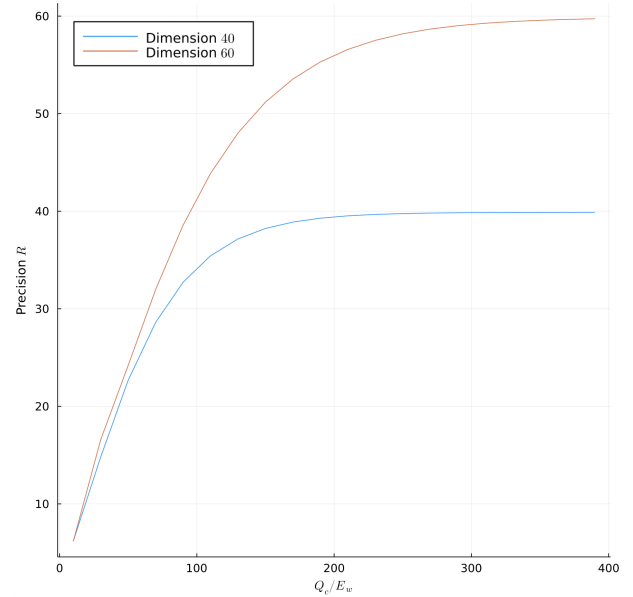


FIG. 7. Precision as a function of Q_c/E_w for two distinct fixed dimensions d .

“ticking” of said clockwork—thus identifying the light-matter system with a quantum clock—we were able to find a light-matter realisation of the quasi-ideal clock. This constitutes the first such realisation and proves that it is at least in-principle realisable. Prior to this work, only semi-classical clocks [11, 12] had been experimentally realised [13, 14] and doubts on whether the appropriate dynamical semi-group for the quasi-ideal clock could be constructed from a physical environment. Here

we have proven that no exotic environments are required and derived from 1st principles the appropriate dynamical semi-group from the physics of light-matter interactions.

The electromagnetic environment we use is the typical isotropic thermal state used to derive standard spontaneous emission. Therefore our approach should be contrasted to those in which the electromagnetic field is altered in some way, such as when it is placed in a cavity, which breaks isotropicity. This can also result in a non-conventional waiting time for a spontaneously emitted photon from an atom in the cavity. A classic example of this is the James-Cummings model [15]. Since the realisation of spontaneous emission is already the best possible under the Markovian light-matter interaction assumption, the only way such anisotropies could enhance it further would be if they introduced a memory effect into the environment making its interaction with the matter non-Markovian. Our work is also identifying a distinct phenomena to that of superadiance and subradiance [16]. Among other things, while both phenomena rely on interference effects of the excited matter, these super and sub radiance effects occur in the many photon-emitter regime, where as ours occurs at the single photon-emitter level.

To derive the dynamical semi-group of the quasi-ideal clock from first principles we needed to overcome two main obstacles: avoidance of decay in the energy basis and careful engineering of the dipole moments coupling the light to matter. The former was achieved by slow oscillations in the excited state while the latter by matter in a ring geometry which induced Berry phases into the dipole moments.

Of course, while our physical derivation of a light-

matter quasi-ideal clock demonstrates that it is in-principle possible, in practice it will likely be hard. One possible approach is to use graphene rings where the flux loop insertion has already been achieved and studied in detail [17]. What is more, other implementations might also be a possibility: the circular geometry which was used to induce the Berry phases in the dipole elements might be realisable via other methods. For example, the crystalline structures satisfying Bloch's theorem which are long enough so that finite boundary effects are not observable, might allow for the necessary symmetries of the dipole couplings (eq. (12)) to be realisable.

Going forward we envisage that our ultra-regular spontaneous emission source can be used to produce ultra-precise photon-delay systems: The activation of the clock can be achieved by a sudden splitting of the excited energy levels, which then produces an emitted photon and change in charge at a chosen time delay at the quantum limit of precision. The research to achieve time delayed photonic emitters is well underway (see [18] and papers here in), but while the precision achieved in [18] represents an unprecedented control of the emission time statistics, it is still far below the ultimate limit proposed in this paper.

ACKNOWLEDGMENTS

We thank Christopher T. Chubb with help running our code for the numerics on to the ETH Zurich Euler computing cluster. M.P.W. was supported by an Ambizione fellowship from the Swiss National Science Foundation (grant No. PZ00P2_179914) in addition to the NCCR QSIT.

Appendix A: Derivation of the master equation for the clockwork

In this appendix we will derive the master equation corresponding to our experimental proposal. We will clearly layout and justify the approximations we make, which are standard in the literature. This appendix is divided into two subsections. The first is standard in the literature and is included for completeness and to fix notation while the second is coublong specific to our setup.

1. Generic open quantum system part of the derivation

Here we will go from a Hamiltonian description of the system and bath, to the description just before the RWA is typically performed. It will be a completely standard textbook derivation for light-matter interactions (indeed it can be found in e.g. [19, 20]). The only small specific specialisation to our particular light-matter interaction will be the choice of spectrum of the matter in eq. (A14).

Consider the Hamiltonian on the system and bath of the form

$$H(t) = H_S \otimes \mathbb{1}_B + \mathbb{1}_S \otimes H_B + H_{SB}(t), \quad (\text{A1})$$

where H_S , H_B are the Hamiltonians of the system and bath respectively, and $H_{SB}(t)$ is a (potentially time-dependent) interaction term coupling the dynamics of the system and bath. We will proceed by going into the interaction picture. For this we need to defined the unitaries $U_0(t)$, $U(t)$ via the solution to a differential equation: that of the free

dynamics and that of the total dynamics

$$\frac{d}{dt}U_0(t) = -i(H_S \otimes \mathbb{1}_B + \mathbb{1}_S \otimes H_B)U_0(t), \quad \frac{d}{dt}U(t) = -iH(t)U(t) \quad (\text{A2})$$

respectively, with initial conditions $U_0(0) = \mathbb{1}_{SB}$, $U(0) = \mathbb{1}_{SB}$. With these two definitions, we can define the dynamics of density operators and observables in the interaction picture by the relations

$$\rho_{SB}^I(t) = U_I(t)\rho_{SB}U_I^\dagger(t), \quad A_I(t) = U_0(t)A_{SB}U_0^\dagger(t), \quad (\text{A3})$$

where

$$U_I(t) := U_0^\dagger(t)U(t) \quad (\text{A4})$$

and ρ_{SB} , A_{SB} are the initial system-bath states and operators respectively.

It follows that

$$\frac{d}{dt}U_I(t) = -i\bar{H}_I(t)U_I(t), \quad (\text{A5})$$

where we have defined the interaction picture interaction term as $\bar{H}_I(t) := U_0^\dagger(t)H_{SB}(t)U_0(t)$. Therefore,

$$\frac{d}{dt}\rho_{SB}^I(t) = -i[\bar{H}_I(t), \rho_{SB}^I(t)], \quad (\text{A6})$$

yielding the solution

$$\rho_{SB}^I(t) = \rho_{SB}^I(0) - i \int_0^t dt [\bar{H}_I(t), \rho_{SB}^I(t)] = \rho_{SB} - i \int_0^t dt [\bar{H}_I(t), \rho_I(t)]. \quad (\text{A7})$$

Substituting the above equation into eq. (A6) and tracing out the bath yields

$$\frac{d}{dt}\rho_S^I(t) = - \int_0^t ds \text{tr}_B [\bar{H}_I(t), [\bar{H}_I(s), \rho_{SB}^I(s)]], \quad (\text{A8})$$

where $\rho_S^I(t) := \text{tr}_B \rho_{SB}^I(t)$ and we have made our first assumption, namely that

$$\text{tr}_B [\bar{H}_I(t), \rho_{SB}] = 0. \quad (\text{A9})$$

We will now make two more assumptions. Our second assumption is that the so-called Born approximation holds. This assumption states that

$$\rho_{SB}^I(s) \approx \rho_S^I(s) \otimes \rho_B. \quad (\text{A10})$$

This assumption is reasonable when environmental excitations decay over times which are not resolved. This assumption is called the Markov approximation and is our third assumption. It consists in replacing $\rho_S^I(s)$ with $\rho_S^I(t)$. Together, these two approximations are known as the Born-Markov approximation and yield the following differential equation when substituting into eq. (A8)

$$\frac{d}{dt}\rho_S^I(t) = - \int_0^t ds \text{tr}_B [\bar{H}_I(t), [\bar{H}_I(s), \rho_S^I(t) \otimes \rho_B]]. \quad (\text{A11})$$

Finally, there is one more assumption needed in order to turn the above equation into a dynamical semi-group: we must replace s by $s - t$ and replace the upper integral limit t by $+\infty$. This approximation is permissible when the integrand disappears sufficiently fast for $s \gg \tau_B$, where τ_B is the time-scale over which the reservoir correlation functions decay.

$$\frac{d}{dt}\rho_S^I(t) = - \int_0^\infty ds \text{tr}_B [\bar{H}_I(t), [\bar{H}_I(s-t), \rho_S^I(t) \otimes \rho_B]]. \quad (\text{A12})$$

The interaction term $H_{SB}(t)$ is expanded as a sum of product terms between Hermitian system operators $H_{SB}(t) = \vec{D} \cdot \vec{E} = \sum_{\alpha \in \{x,y,z\}} D_\alpha \otimes E_\alpha$, where $D_\alpha = q \hat{r}_\alpha$. We are using the convention that the dipole vector $q(\hat{r}_x, \hat{r}_y, \hat{r}_z)$ points

in the direction of positive change. In our setup, $q(\hat{r}_x, \hat{r}_y, \hat{r}_z) = q(0, 0, \hat{r}_z)$ since the changes are centred around the z -axis. However, it is insightful to not assume this now, as derive a more general condition for our clock to work. This generality could account for, e.g. a small misalignment of the change distribution so that the x and y components are not exactly zero. We now expand the dipole moment operator D_z in terms of eigenspaces of the free system Hamiltonian H_S . Let $\{\varepsilon\}$ be the set of eigenvalues of H_S . Let $\pi(\varepsilon)$ be the projector onto eigenstate corresponding to eigenvalue ε . Since the summation over said projectors is a resolution of the identity, we have that

$$H_{\text{SB}}(t) = \sum_{\alpha} \sum_{\varepsilon, \varepsilon'} \pi(\varepsilon) D_{\alpha} \pi(\varepsilon') \otimes E_{\alpha} = \sum_{\alpha} \sum_{\omega} D_{\alpha}(\omega) \otimes E_{\alpha}, \quad (\text{A13})$$

where $D_{\alpha}(\omega) := \sum_{\varepsilon' - \varepsilon = \omega} \pi(\varepsilon) D_{\alpha} \pi(\varepsilon')$. In particular, since H_S has evenly spaced eigenvalues, $\varepsilon = \omega_0 n$ ($n \in \{0, 1, \dots, d-1\}$) and ω takes all values of the set

$$\{\pm n\omega_0, \pm(\omega_{0m} + n\omega_0) : n = 0, 1, \dots, d-1\}, \quad (\text{A14})$$

where recall ω_0 is the frequency of the harmonic oscillator Hamiltonian eq. (7) and ω_{0m} is the energy gap between the ground state of the oscillator, $|E_0\rangle$, and the secondary ring $|2^{\text{ndry}}, m\rangle$. The $\omega = 0$ case corresponds to same-energy-state coupling, which will not play a role as we will see. Meanwhile, the $\pm n\omega_0$ terms correspond to inter-primary-ring transitions which are dipole-forbidden (as discussed in the main text) and the terms $\omega_{0m} + n\omega_0$ are responsible for transitions from primary to secondary rings and the terms $-(\omega_{0m} + n\omega_0)$ reverse process.

We thus find

$$\bar{H}_I(t) = U_0^\dagger(t) \left(\sum_{\omega, \alpha} D_{\alpha}(\omega) \otimes E_{\alpha} \right) U_0(t) = \sum_{\omega, \alpha} e^{-i\omega t} D_{\alpha}(\omega) \otimes E_{\alpha}(t) = \sum_{\omega, \alpha} e^{i\omega t} D_{\alpha}^\dagger(\omega) \otimes E_{\alpha}(t), \quad (\text{A15})$$

where $E_{\alpha}(t) := e^{itH_B} E_{\alpha} e^{-itH_B}$. Therefore, plugging into eq. (A12) we find

$$\frac{d}{dt} \rho_S^I(t) = - \int_0^\infty ds \text{tr}_B \left[\bar{H}_I(t-s) \rho_S^I(t) \otimes \rho_B \bar{H}_I(t) - \bar{H}_I(t) \bar{H}_I(t-s) \rho_S^I(t) \otimes \rho_B \right] + \text{h.c.} \quad (\text{A16})$$

$$= \sum_{\alpha, \alpha'} \sum_{\omega, \omega'} e^{it(\omega' - \omega)} \Gamma_{\alpha, \alpha'}(\omega) \left(D_{\alpha}(\omega) \rho_S^I(t) D_{\alpha'}^\dagger(\omega') - D_{\alpha'}^\dagger(\omega') D_{\alpha}(\omega) \rho_S^I(t) \right) + \text{h.c.}, \quad (\text{A17})$$

where

$$\Gamma_{\alpha, \alpha'}(\omega) := \int_0^\infty ds e^{i\omega s} \text{tr}_B \left[E_{\alpha'}^\dagger(t) E_{\alpha}(t-s) \rho_B \right] = \int_0^\infty ds e^{i\omega s} \text{tr}_B \left[E_{\alpha'}^\dagger(s) E_{\alpha}(0) \rho_B \right], \quad (\text{A18})$$

and in the last line we have used the fact that ρ_B is a Gibbs state and thus is stationary w.r.t. the free Hamiltonian of the bath, H_B .

We can now simplify our first assumption, namely eq. (A9), to find

$$\text{tr}_B \left[\left(\sum_{\omega, \alpha} e^{-i\omega t} D_{\alpha}(\omega) \otimes E_{\alpha}(t) \right), \rho_S \otimes \rho_B \right] = 0, \quad (\text{A19})$$

which is implied by

$$\text{tr} E_{\alpha} \rho_B = 0, \quad \forall \alpha \in \{x, y, z\} \quad (\text{A20})$$

when the above mentioned stationary of ρ_B is taken into account.

2. Special dipole moment symmetries

In this section we will complete the derivation of our dynamical semigroup which was started in the previous section. We will specialise to our setup by using the symmetry in the dipole moments and frequency rage it provides.

For a thermal bath, in which we neglect the imaginary part of $\Gamma(\omega)$ we have

$$\Gamma_{\alpha, \alpha'}(\omega) = \Gamma(\omega) \delta_{\alpha, \alpha'}, \quad \Gamma(\omega) = \frac{2\omega^3}{3c^3} (1 + N(\omega)). \quad (\text{A21})$$

When $\omega > 0$, $N(\omega)$ is the number of photons with frequency ω in the Fock space and given by the Planck distribution. The terms give rise to photo emission and the clock ticking. The $\omega < 0$ case correspond to the reverse process and it is convenient to use the identity $N(\omega) = -(1 + N(-\omega))$ to write the decay coefficient as

$$\Gamma(-\omega) = \frac{2\omega^3}{3c^3} N(\omega). \quad (\text{A22})$$

As discussed and motivated in section III B and recall $\{\alpha, \alpha'\} \in \{x, y, z\}$. Therefore, plugging into eq. (A16), we find

$$\begin{aligned} \frac{d}{dt} \rho_S^I(t) &= \sum_{\alpha} \sum_{\omega, \omega' > 0} e^{it(\omega' - \omega)} \Gamma(\omega) \left(D_{\alpha}(\omega) \rho_S^I(t) D_{\alpha}^{\dagger}(\omega') - D_{\alpha}^{\dagger}(\omega') D_{\alpha}(\omega) \rho_S^I(t) \right) + \text{h.c.}, \\ &+ \sum_{\alpha} \sum_{\omega, \omega' > 0} e^{-it(\omega' - \omega)} \Gamma(-\omega) \left(D_{\alpha}^{\dagger}(\omega) \rho_S^I(t) D_{\alpha}(\omega') - D_{\alpha}(\omega') D_{\alpha}^{\dagger}(\omega) \rho_S^I(t) \right) + \text{h.c.} \\ &+ \sum_{\alpha} \left(\sum_{\omega > 0, \omega' < 0} + \sum_{\omega < 0, \omega' > 0} \right) e^{it(\omega' - \omega)} \Gamma(\omega) \left(D_{\alpha}(\omega) \rho_S^I(t) D_{\alpha}^{\dagger}(\omega') - D_{\alpha}^{\dagger}(\omega') D_{\alpha}(\omega) \rho_S^I(t) \right) + \text{h.c.}, \end{aligned} \quad (\text{A23})$$

where we have used $D_{\alpha}(-\omega) = D_{\alpha}^{\dagger}(\omega)$. The only relevant frequencies from eq. (A14) are $\omega = \pm(\omega_{0m} + n\omega_0)$, $n \in \{0, 1, \dots, d-1\}$, as all the others are either dipole-forbidden or do not appear in eq. (A23). Recalling the identity $\omega_{0m} \gg (d-1)\omega_0$, we thus see that $|\omega' - \omega|$ in the exponential of the last line is much larger than the same term in the first and second lines. These oscillations are occurring on a much faster timescale than the relaxation time of the system, and hence we can invoke the rotation wave approximation to eliminate the last line of eq. (A23). However, the rotating wave approximation is invalid for the first and second lines, since the average time it take for the clock to tick corresponds to about half a rotation. We thus have

$$\begin{aligned} \frac{d}{dt} \rho_S^I(t) &= \sum_{\alpha} \sum_{\omega, \omega' > 0} e^{it(\omega' - \omega)} \Gamma(\omega) \left(D_{\alpha}(\omega) \rho_S^I(t) D_{\alpha}^{\dagger}(\omega') - D_{\alpha}^{\dagger}(\omega') D_{\alpha}(\omega) \rho_S^I(t) \right) \\ &+ \sum_{\alpha} \sum_{\omega, \omega' > 0} e^{-it(\omega' - \omega)} \Gamma(-\omega) \left(D_{\alpha}^{\dagger}(\omega) \rho_S^I(t) D_{\alpha}(\omega') - D_{\alpha}(\omega') D_{\alpha}^{\dagger}(\omega) \rho_S^I(t) \right) + \text{h.c.} \end{aligned} \quad (\text{A24})$$

For the remaining relevant frequencies, we have

$$D_{\alpha}(-(\omega_{0m} + n\omega_0)) = D_{\alpha}^{\dagger}(\omega_{0m} + n\omega_0), \quad D_{\alpha}(\omega_{0m} + n\omega_0) = a_{n\alpha}^{(m)} |2^{\text{ndry}}, m\rangle \langle E_n|, \quad (\text{A25})$$

with $a_{n\alpha}^{(m)} := q \langle E_n | \hat{\alpha} | 2^{\text{ndry}}, m \rangle$. We now make the assumption that

$$a_{n\alpha}^{(m)} = e^{\frac{i2\pi n m}{d}} e^{i\theta_{\alpha, m}} |a_{n\alpha}^{(m)}|, \quad (\text{A26})$$

where $\theta_{\alpha, m} \in \mathbb{R}$. This clearly holds in our setup, due to eq. (12). However, it is informative to only assume the weaker assumption eq. (A26) for now as this way we can derive a more general condition on the dipole coupling which may be useful if the geometry is not identical to that described. E.g. if there were an imperfection such as the rings not being perfectly perpendicular, and the coupling strength in one of the wells of the primary ring is slightly stronger than that of the other wells. Substituting eq. (A25) into eq. (A24) and using assumption eq. (A26), we arrive at

$$\begin{aligned} \frac{d}{dt} \rho_S^I(t) &= \sum_{\alpha} \sum_{n, n'=0}^{d-1} e^{it\omega_0(n' - n)} \Gamma(\omega_{0m} + n\omega_0) \left(D_{\alpha}(\omega_{0m} + n\omega_0) \rho_S^I(t) D_{\alpha}^{\dagger}(\omega_{0m} + n'\omega_0) - D_{\alpha}^{\dagger}(\omega_{0m} + n'\omega_0) D_{\alpha}(\omega_{0m} + n\omega_0) \rho_S^I(t) \right) \\ &+ \sum_{\alpha} \sum_{n, n'=0}^{d-1} e^{it\omega_0(n - n')} \Gamma(-(\omega_{0m} + n\omega_0)) \left(D_{\alpha}^{\dagger}(\omega_{0m} + n\omega_0) \rho_S^I(t) D_{\alpha}(\omega_{0m} + n'\omega_0) - D_{\alpha}(\omega_{0m} + n'\omega_0) D_{\alpha}^{\dagger}(\omega_{0m} + n\omega_0) \rho_S^I(t) \right) \\ &+ \text{h.c.} \\ &= \sum_{\alpha} \sum_{n, n'=0}^{d-1} e^{it\omega_0(n' - n)} \Gamma(\omega_{0m} + n\omega_0) |a_{n\alpha}^{(m)} a_{n'\alpha}^{(m)}| e^{i2\pi(n - n')m/d} \left(\langle E_n | \rho_S^I(t) | E_{n'} \rangle |2^{\text{ndry}}, m\rangle \langle 2^{\text{ndry}}, m| - |E_{n'}\rangle \langle E_n| \rho_S^I(t) \right) \\ &+ \sum_{\alpha} \sum_{n, n'=0}^{d-1} e^{it\omega_0(n - n')} \Gamma(-(\omega_{0m} + n\omega_0)) |a_{n'\alpha}^{(m)} a_{n\alpha}^{(m)}| e^{i2\pi(n' - n)m/d} \left(\langle 2^{\text{ndry}}, m | \rho_S^I(t) | 2^{\text{ndry}}, m \rangle |E_n\rangle \langle E_{n'}| \right. \\ &\quad \left. - \delta_{n, n'} |2^{\text{ndry}}, m\rangle \langle 2^{\text{ndry}}, m| \rho_S^I(t) \right) + \text{h.c.} \end{aligned} \quad (\text{A27})$$

Now, let us assume there exists $C_0 > 0$ independent of n such that

$$\sum_{\alpha} \Gamma(\omega_{0m} + n\omega_0) \left| a_{n\alpha}^{(m)} a_{n'\alpha}^{(m)} \right| = C_0^{(m)}, \quad \forall n, n' \in \{0, 1, \dots, d-1\}. \quad (\text{A28})$$

We justify physically in appendix A3. Furthermore, we will see that when it is satisfied approximately, then to a good approximation we also have

$$\sum_{\alpha} \Gamma(-(\omega_{0m} + n\omega_0)) \left| a_{n\alpha}^{(m)} a_{n'\alpha}^{(m)} \right| = C_0'^{(m)}, \quad \forall n, n' \in \{0, 1, \dots, d-1\}. \quad (\text{A29})$$

from eq. (A27) it follows

$$\begin{aligned} \frac{d}{dt} \rho_S^{\text{I}}(t) &= C_0^{(m)} d \left(\langle t_m(t) | \rho_S^{\text{I}}(t) | t_m(t) \rangle | 2^{\text{ndry}}, m \rangle \langle 2^{\text{ndry}}, m | - | t_m(t) \rangle \langle t_m(t) | \rho_S^{\text{I}}(t) \right) \\ &\quad + C_0'^{(m)} d \left(\langle 2^{\text{ndry}}, m | \rho_S^{\text{I}}(t) | 2^{\text{ndry}}, m \rangle | t_m(t) \rangle \langle t_m(t) | - | 2^{\text{ndry}}, m \rangle \langle 2^{\text{ndry}}, m | \rho_S^{\text{I}}(t) \right) \\ &\quad + \text{h.c.} \\ &= \hat{J}_m(t) \rho_S^{\text{I}}(t) \hat{J}_m^\dagger(t) - \frac{1}{2} \left\{ \hat{J}_m^\dagger(t) \hat{J}_m(t), \rho_S^{\text{I}}(t) \right\} \\ &\quad + \hat{L}_m(t) \rho_S^{\text{I}}(t) \hat{L}_m^\dagger(t) - \frac{1}{2} \left\{ \hat{L}_m^\dagger(t) \hat{L}_m(t), \rho_S^{\text{I}}(t) \right\} \end{aligned} \quad (\text{A30})$$

where in the first line we have defined $|t_m(t)\rangle := e^{itH_C} |t_m\rangle$, with $|t_m\rangle$ the m^{th} basis element of the quantum Fourier transform given by eq. (9) and H_C is the clockwork Hamiltonian eq. (7). In the last lines, we have defined

$$\hat{J}_m(t) := e^{itH_S} \hat{J}_m e^{-itH_S} = \sqrt{2dC_0^{(m)}} |2^{\text{ndry}}, m\rangle \langle t_m(t)|, \quad \hat{J}_m := \sqrt{2dC_0^{(m)}} |2^{\text{ndry}}, m\rangle \langle t_m|, \quad (\text{A31})$$

$$\hat{L}_m(t) := e^{itH_S} \hat{L}_m e^{-itH_S} = \sqrt{2dC_0'^{(m)}} (|2^{\text{ndry}}, m\rangle \langle t_m(t)|)^\dagger, \quad \hat{L}_m := \sqrt{2dC_0'^{(m)}} (|2^{\text{ndry}}, m\rangle \langle t_m|)^\dagger, \quad (\text{A32})$$

where recall H_S is the total matter system Hamiltonian defined in eq. (13).

Finally, we can easily generalise this to L secondary rings. Since all the secondary rings are non degenerate, there is no inter-secondary-ring coupling and we merely have to add an extra summation over the secondary rings or in other words, L decay channels. From eq. (A30) we find

$$\begin{aligned} \frac{d}{dt} \rho_S^{\text{I}}(t) &= \sum_{j=1}^L \hat{J}_{m_j}(t) \rho_S^{\text{I}}(t) \hat{J}_{m_j}^\dagger(t) - \frac{1}{2} \left\{ \hat{J}_{m_j}^\dagger(t) \hat{J}_{m_j}(t), \rho_S^{\text{I}}(t) \right\} \\ &\quad \sum_{j=1}^L \hat{L}_{m_j}(t) \rho_S^{\text{I}}(t) \hat{L}_{m_j}^\dagger(t) - \frac{1}{2} \left\{ \hat{L}_{m_j}^\dagger(t) \hat{L}_{m_j}(t), \rho_S^{\text{I}}(t) \right\}. \end{aligned} \quad (\text{A33})$$

Now that we have derived the master equation in the Interaction picture, we can convert back to the Schrödinger picture. Recalling eqs. (A3) and (A4) and denoting the state evolution in the Schrödinger picture by $\rho_{\text{SB}}(t)$, we find

$$\rho_{\text{SB}}(t) := U(t) \rho_{\text{SB}} U^\dagger(t) = U_0(t) \rho_{\text{SB}}^{\text{I}}(t) U_0^\dagger(t). \quad (\text{A34})$$

Therefore, defining $\rho_S(t) := \text{tr}_B[\rho_{\text{SB}}(t)]$ and recalling $\rho_S^{\text{I}}(t) := \text{tr}_B \rho_{\text{SB}}^{\text{I}}(t)$, it follows

$$\rho_S(t) = e^{-itH_S} \text{tr}_B [e^{-itH_B} \rho_{\text{SB}}^{\text{I}}(t) e^{itH_B}] e^{itH_S} = e^{-itH_S} \rho_S^{\text{I}}(t) e^{itH_S}, \quad (\text{A35})$$

where we used the cyclicity of the trace. Furthermore, from eq. (A34) it also follows

$$\frac{d}{dt} \rho_{\text{SB}}(t) = -i[H_S, \rho_{\text{SB}}(t)] - i[H_B, \rho_{\text{SB}}(t)] + U_0(t) \left(\frac{d}{dt} \rho_{\text{SB}}^{\text{I}}(t) \right) U_0^\dagger(t) \quad (\text{A36})$$

Thus

$$\begin{aligned} \frac{d}{dt} \rho_S(t) &= \text{tr}_B \left[\frac{d}{dt} \rho_{\text{SB}}(t) \right] = -i[H_S, \rho_S(t)] + e^{-itH_S} \text{tr}_B \left[\frac{d}{dt} \rho_{\text{SB}}^{\text{I}}(t) \right] e^{itH_S} \\ &= -i[H_S, \rho_S(t)] + \sum_{j=1}^L \hat{J}_{m_j} \rho_S(t) \hat{J}_{m_j}^\dagger - \frac{1}{2} \left\{ \hat{J}_{m_j}^\dagger \hat{J}_{m_j}, \rho_S(t) \right\} \\ &\quad + \sum_{j=1}^L \hat{L}_{m_j} \rho_S(t) \hat{L}_{m_j}^\dagger - \frac{1}{2} \left\{ \hat{L}_{m_j}^\dagger \hat{L}_{m_j}, \rho_S(t) \right\}, \end{aligned} \quad (\text{A37})$$

where we have used the cyclicity of the trace and the first line and eqs. (A8) and (A33) in the second.

Physically, the second line of eq. (A37) corresponds to spontaneous emission of a photon and the change jumping from the primary ring to a secondary ring, while the third line correspond to the reverse process. Since we identify a tick as the emission of a photon, and we assume that this process is detectable to us (either by detecting the emitted photon or the change in charge in the rings), we can make the register where this information is stored explicit. We do not associate the reverse process with a tick. This corresponds to the mapping

$$J_{m_j} \rightarrow \tilde{J}_{m_j} := J_{m_j} \otimes O_{\mathbb{R}}, \quad (\text{A38})$$

$$L_{m_j} \rightarrow \tilde{L}_{m_j} := L_{m_j} \otimes \mathbb{1}_{\mathbb{R}}, \quad (\text{A39})$$

where $O_{\mathbb{R}} := |1\rangle\langle 0|_{\mathbb{R}} + |2\rangle\langle 1|_{\mathbb{R}} + |3\rangle\langle 2|_{\mathbb{R}} + \dots + |N_T\rangle\langle N_T - 1|_{\mathbb{R}}$ advances the classical register by one every time there is a spontaneous emission and $\mathbb{1}_{\mathbb{R}}$ is the identity operator. Performing this mapping on eq. (A37) gives

$$\begin{aligned} \frac{d}{dt}\rho_{\text{SR}}(t) = & -i[H_{\text{S}}, \rho_{\text{SR}}(t)] + \sum_{j=1}^L \tilde{J}_{m_j} \rho_{\text{SR}}(t) \tilde{J}_{m_j}^\dagger - \frac{1}{2} \left\{ \tilde{J}_{m_j}^\dagger \tilde{J}_{m_j}, \rho_{\text{SR}}(t) \right\} \\ & + \sum_{j=1}^L \tilde{L}_{m_j} \rho_{\text{SR}}(t) \tilde{L}_{m_j}^\dagger - \frac{1}{2} \left\{ \tilde{L}_{m_j}^\dagger \tilde{L}_{m_j}, \rho_{\text{SR}}(t) \right\}. \end{aligned} \quad (\text{A40})$$

From eq. (8), we see that we just need to choose $L = d$, and $\{V_j = dC_0^{(m_j)}\}_{j=0}^{d-1}$ with $m_j = j$, we achieve the dynamical semigroup of the quasi-ideal clock if $\{\tilde{L}_j = 0\}_{j=0}^{d-1}$. We will see in the next section, the this is true to a very good approximation in the low bath temperature regime. Physically, this is the regime of interest since the reverse process of spontaneous emission require the absorption of a photon from the bath. Therefore, at low temperatures, this process is highly suppressed since the mean occupancy number of the bath is close to zero, see fig. 4 and next section. Another important point in that in practice we see in fig. 5 that the optimal solution is for most of the V_j coefficients to be zero. This is equivalent to the secondary ring with m_j flux loops being omitted from the setup. So in practice, we need far fewer secondary rings than the theoretical maximum of d .

3. Constraint eq. (A28) and low temperature limit

a. Constraint eq. (A28)

We now return to assumption eq. (A28). Recalling that $\omega_{0m} \gg (d-1)\omega_0$ for all $m \in \{0, 1, \dots, d-1\}$, using eq. (A21) we deduce

$$\Gamma(\omega_{0m} + n\omega_0) = \Gamma(\omega_{0m}) \left(1 + \mathcal{O}\left(n \frac{\omega_0}{\omega_{0m}}\right)^2 \right) \frac{1 + N(\omega_{0m} + n\omega_0)}{1 + N(\omega_{0m})} \approx \Gamma(\omega_{0m}) \quad \forall m, n \in \{0, 1, \dots, d-1\} \quad (\text{A41})$$

Therefore, the assumption eq. (A28) becomes

$$\sum_{\alpha} \left| a_{n\alpha}^{(m)} a_{n'\alpha}^{(m)} \right| \approx C_1^{(m)}, \quad \forall n, n' \in \{0, 1, \dots, d-1\}, \quad (\text{A42})$$

where $C_1^{(m)}$ is a new constant independent of n, n' . To verify that this is indeed satisfied by the setup from the main text, we start by noting that the dipole of secondary ring with m flux loops is $d_m = q_m r_m = q_m(0, 0, z_m \hat{z})$ where \hat{z} is the unit operator for the z -axis and z_m is the location of the secondary ring along said axis. Therefore,

$$a_{n,x}^{(m)} = a_{n,y}^{(m)} = 0, \quad (\text{A43})$$

$$a_{n,z}^{(m)} = q_m \langle E_n | z_m \hat{z} | 2^{\text{ndry}}, m \rangle = q_m e^{i2\pi n m/d} a_{0,z}^{(m)} \quad n, m \in \{0, 1, \dots, d-1\} \quad (\text{A44})$$

and thus inserting into eq. (A42) we find that $C_1^{(m)}$ is n, n' independent as required.

Finally we want to verify that eq. (A29) is also satisfied. This condition is the same as eq. (A28) up to a change of $\Gamma(\omega_{0m} + n\omega_0)$ for $\Gamma(-(\omega_{0m} + n\omega_0))$. From eq. (A22) and using that $\omega_{0m} \gg (d-1)\omega_0$ we also find that

$$\Gamma(-(\omega_{0m} + n\omega_0)) = \Gamma(-\omega_{0m}) \left(1 + \mathcal{O}\left(n \frac{\omega_0}{\omega_{0m}}\right)^2 \right) \frac{N(\omega_{0m} + n\omega_0)}{N(\omega_{0m})} \approx \Gamma(-\omega_{0m}) \quad \forall m, n \in \{0, 1, \dots, d-1\}, \quad (\text{A45})$$

thus eq. (A29) is also satisfied.

b. *Low temperature limit*

Since the bath is in a thermal state (formally a Gibbs state). The mean occupation number of the bath decreases rapidly with the temperature of the thermal state, therefore at low temperatures $N(\omega_{0m}) \approx 0$. Therefore in this limit we observe from eqs. (A21) and (A22) that

$$\Gamma(\omega_{0m}) \approx \frac{2\omega_{0m}^3}{3c^3}, \quad \Gamma(-\omega_{0m}) \approx 0. \quad (\text{A46})$$

Thus $C_0^{(m)} > 0$ and relatively large, while $C_0^{\prime(m)} \approx 0$. Therefore, from the definition of $\{\hat{J}_m, \hat{L}_m\}$ in eq. (A31) we see that the last line of eq. (A37) is approximately zero and thus we realise the quasi-ideal clock in this low temperature limit.

Appendix B: Lifting the degeneracy of the primary ring

We consider a ring with radius R and parameterize it with a coordinate $x \in [0, 2\pi R)$. Prior to activating the clock, we start with d evenly spaced wells, that is with a potential of the form

$$U(x) = \frac{1}{2}m\omega^2(x - \lfloor x/a \rfloor \cdot a - a/2)^2 \text{ for } x \in [0, 2\pi R), \quad a = \frac{2\pi R}{d}$$

For sufficiently large ω or R we have d degenerate ground states. In the following we fix $R = 1$ and assume that ω is sufficiently large, i.e., we work in the tight-binding limit of a lattice with d atoms and periodic boundary conditions.

1. Identification of Blochwave and t_k

Observe that if the wave function of the ground state is $\psi_0(x)$ the discrete Fourier transformer looks like

$$\langle x | t_k \rangle = \frac{1}{d} \sum_{n=0}^{d-1} e^{-\frac{2\pi i n k}{d}} \psi_0(x - an - \frac{a}{2}) = \frac{1}{d} \sum_{n=0}^{d-1} e^{-ian \cdot k} \psi_0(x - an - \frac{a}{2}). \quad (\text{B1})$$

for $k \in \{0, \dots, d-1\}$. This reminds us of Bloch wave functions. In fact, by Bloch's theorem any single particle wave function that is a solution to this a periodic potential can be written as $\psi_p(x) = e^{ipx} u_p(x)$ for p in $[0, 2\pi/a)$ and u_p being a periodic, i.e., $u_p(x) = u_p(x + a)$. As we have periodic boundary conditions (Born-von Karman boundary conditions) we have that $p = \frac{2\pi}{da} k$ for $k \in 0, \dots, d-1$. Thus, the tight-binding wave functions of the ground states have the form

$$\psi_p(x) = e^{ipx} \frac{1}{d} \sum_{n=0}^{d-1} \psi_0(x - an - \frac{a}{2}). \quad (\text{B2})$$

As the wave function $\psi_p(x)$ has only reasonable support near the potential minima, i.e., for $x = na + a/2 + y$ $n \in 0, \dots, d-1$ and approximately $-a/2 < y < a/2$. Thus the factor e^{ipx} add the phase $e^{ipx} = e^{ipna} e^{ipa/2} e^{ipy}$ to the wave function at the n th well. Using $p = \frac{2\pi}{da} k$ yields $e^{ipx} = e^{\frac{2\pi i k n}{d}} (-1)^k e^{\frac{2\pi i k y}{da}}$. The factor $(-1)^k$ is just a gauge and because y is small compared to da we can motivate the identification of t_k with the tight-binding wave function of the groundstate with quasi momentum k .

2. The harmonic potential

Now we want to add a perturbation $V(x)$ to $U(x)$ that leads to a harmonic oscillator Hamiltonian. Any potential on this ring can be written as

$$\hat{V} = \int_0^{2\pi} dx V(x) |x\rangle\langle x|. \quad (\text{B3})$$

We define the orthonormal Fourier basis $\langle x|k\rangle = \frac{e^{ikx}}{\sqrt{2\pi}}$ for $k \in \mathbb{Z}$. Further, we can expand $V(x) = \sum_{q \in \mathbb{N}_0} V_q e^{iqx} + h.c.$. In total, we get

$$\hat{V} = \int_0^{2\pi} |x\rangle\langle x| = \sum_{q \in \mathbb{N}_0} V_q \int_0^{2\pi} dx e^{iqx} |x\rangle\langle x| + h.c. \quad (\text{B4})$$

$$= \sum_{k,l,q \in \mathbb{N}_0} V_q \frac{1}{2\pi} \int_0^{2\pi} dx e^{ix(q+l-k)} |k\rangle\langle l| + h.c. = \sum_{q,l \in \mathbb{N}_0} V_q |l+q\rangle\langle l| + h.c. \quad (\text{B5})$$

By the above (recall $2\pi/(da) = 1$) we can to a good approximation identify the $|l\rangle$ states with $|t_l\rangle$ states. Consequently, we will compare this form to the harmonic oscillator Hamiltonian in the time basis to get the perturbation. Using that the energy eigenstates $|n\rangle = \frac{1}{\sqrt{d}} \sum_{k=0}^{d-1} e^{2\pi i kn/d} |t_k\rangle$ and that $H = \sum_{n=0}^{d-1} \omega_0 n |E_n\rangle\langle E_n|$, we get

$$H = \sum_{n=0}^{d-1} \omega_0 n |E_n\rangle\langle E_n| = \omega_0 \sum_{n,k=0}^{d-1} \frac{n}{\sqrt{d}} e^{\frac{2\pi i nk}{d}} |t_k\rangle\langle E_n| \quad (\text{B6})$$

$$= \omega_0 \sum_{n,k,l=0}^{d-1} \frac{n}{d} e^{\frac{2\pi i (k-l)n}{d}} |t_k\rangle\langle t_l| \quad (\text{B7})$$

$$= \omega_0 \sum_{q=0}^{d-1} \sum_{k=0}^{d-1} |t_{k+1}\rangle\langle t_k| \sum_{n=0}^{d-1} \frac{n}{d} e^{\frac{2\pi i n(k-l)}{d}} \quad (\text{B8})$$

$$= \omega_0 \sum_{q=0}^{d-1} \sum_{k=0}^{d-1} |t_{k+q}\rangle\langle t_k| \left(\delta_{q,0} \frac{1}{d} \frac{d(d-1)}{2} + (1 - \delta_{0,q}) \frac{1}{d} \frac{1}{e^{\frac{2\pi i q}{d}} - 1} \right) \quad (\text{B9})$$

Importantly, the terms in brackets in the last line are k -independent. Thus, comparing this expression with Eq. B5 we get $V_q = \frac{1}{e^{\frac{2\pi i q}{d}} - 1}$ for $q \in 1, \dots, d-1$ and $V_0 = (d-1)/2$. In fact, V_0 is only a constant shift, so we can drop this term.

Transforming this expression back to real space by $V(x) = \sum_q V_q e^{iqx} + h.c.$ using

$$\frac{1}{e^{\frac{2\pi i q}{d}} - 1} = -\frac{1}{2} - \frac{i}{2} \frac{\sin(\frac{2\pi q}{d})}{1 - \cos(\frac{2\pi q}{d})}$$

yields $V(x) = (d-1) + \sum_{q=1}^{d-1} -\cos(qx) + \frac{\sin(\frac{2\pi q}{d})}{1 - \cos(\frac{2\pi q}{d})} \sin(qx)$. Numerically, it was successfully checked that the potential $V(x) + U(x)$ in the tight binding approximation (large ω) yields a harmonic splitting in the spectrum which is well separated from the higher energy states. In a real experiment, one should rather use the first d coefficients V_q and re-optimize them to guarantee harmonic splitting.

3. Numerics on the equal dipole moments

The goal of this appendix is to show numerically that we can operate in a limit in which the matrix elements $|\langle l|\hat{D}|2^{\text{ndry}}, m\rangle|$ are equal for $l \in \{0, \dots, d-1\}$. This is the sufficient condition to mimic the dynamics of the quasi-ideal clock, as can be seen from eq. (A42) (which is the generalisation of eq. (12)). For that, we simply take the potential $V(x) + U(x)$ on the lower ring and solve the Schrödinger equation numerically for the first d eigenstates. Then we fix the lowest energy wave function and compare the $\|\circ\|_{L^2}$ - norm difference of the n th energy eigenstate and the lowest energy shifted by $2\pi R/d \cdot n$. For $\omega = 3000$ this leads to errors:

$d = 2$	0.002	-	-	-	-	-	-
$d = 3$	0.002	0.002	-	-	-	-	-
$d = 4$	0.001	0.002	0.001	-	-	-	-
$d = 5$	0.001	0.002	0.002	0.001	-	-	-
$d = 6$	0.001	0.002	0.002	0.002	0.001	-	-
$d = 7$	0.002	0.001	0.001	0.001	0.001	0.002	-
$d = 8$	0.001	0.001	0.002	0.002	0.002	0.001	0.001

Thus, we observe that the errors are very small. As the dipole operator is bounded, the L^2 - norm does bound the error on matrix element differences.

Appendix C: Multiple ticks

To extend our in-principle experiment to one where the clock state is re-set to the initial state after each tick, we need to implement the transition $|2^{\text{ndry}}, m\rangle \rightarrow |\psi_C\rangle$ instantaneously. However, the state $|\psi_C\rangle$ may require the concatenation of some elementary processes to be constructed, such as a sequence of gates on a quantum computer which would take non-negligible and predictable time. One way to do this in-principle, would be to construct two copies of the clock both with their clockwork initiated to $|\rho_C\rangle$ with the two primary rings in their degenerate ground state. Then initiate one of the clocks by turning on the primary-ring-degeneracy-lifting potential. Upon the clock ticking, the emitted photon activates the primary-ring-degeneracy-lifting potential of the second clock. One now turns off the primary-ring-degeneracy-lifting potential of the first clock and prepares the initial state $|\psi_C\rangle$ on it. This last operation can be performed at an arbitrary time so long as it is significantly before the mean time between ticks μ ; say $\mu/2$. This way, the probability of the state $|\psi_C\rangle$ being prepared on the first clock before the second clock ticking is vanishingly small. We now allow the photon coming from the tick of the secondary clock to activate the primary-ring-degeneracy-lifting potential of the first clock. Repeating the process indefinitely allows for the full implementation of the quasi-ideal clock. The only additional timing this process has required is the ability to regenerate the initial clock state $|\psi_C\rangle$ in the time-window $[0, \mu/2]$. So as long as μ is significantly larger than the average time needed in said preparation, this additional time requirement is effectively negligible. It also only requires a duplication of efforts, since only two classically correlated clocks are required. If the time needed to prepare the initial clockwork state $|\psi_C\rangle$, is larger than μ , one can trivially generalise this scheme to include N copies of the clock, thus having a time window of $[0, (N - 1)\mu]$ in which to prepare each initial clockwork state. This method for re-setting can also be applied to other clockwork systems which require a manual reset, such as the semi-classical clock in [21].

Appendix D: Reproducing the precision per tick in [11] with our definition

Here we show that our definition of entropy per tick eq. (20) which is valid for any clock, reproduces that found in [11] when specialised to the clock model found therein. The clock model in [11] can be parametrised in terms of the entropy per tick $\Delta S'_{\text{tick}}$ which the first tick generates. In fig. 8 we plot the entropy per tick according to eq. (20) as a function of ΔS_{tick} . We observe a perfect straight line with unit gradient demonstrating that the two quantities are indeed equal as claimed.

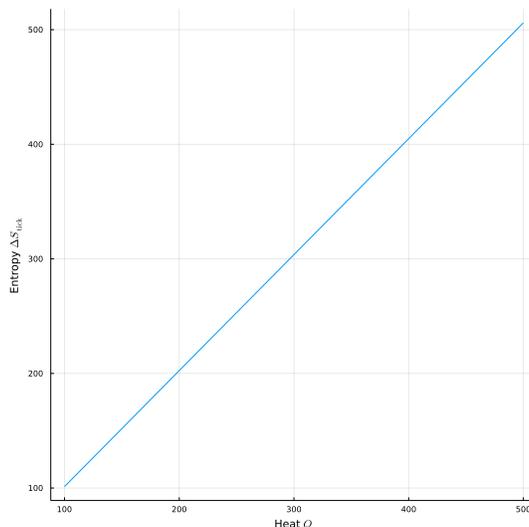


FIG. 8. Entropy per tick as a function of the heat generated by the model (see [11] for model details).

Appendix E: Numerical results

In this section we present a numerical method for calculating the optimal precision of the first tick R in low dimensions. This algorithm was essential to obtaining the data for figs. 2, 4 and 5. To do so, we will derive a

connection between the precision of a clock and a set of Lyapunov equations.

The most elementary and intuitive method to derive the precision of the clock is to solve the dynamics of the clockwork via routine numerical methods for solving dynamical semigroup such as eq. (3). One then calculates the delay function via eq. (5), and finally computes its first and second moments from which R follows via eq. (6). Unfortunately, the higher the precision of the clock, the closer the delay function is to a Dirac delta function which results in numerical instabilities. Using this method, we were unable to accurately compute the precision for $d > 3$. We thus derive a new expression for the accuracy which, unlike eq. (6), does not involve the delay function and is amenable to numerical computation.

With $\hat{V}(t) := e^{(iH_C - \hat{V})t} \hat{V} e^{-(iH_C - \hat{V})t}$, it follows from eq. (5) that we can rewrite the ticking probability as

$$P_{\text{tick}}(t) = 2 \operatorname{tr}(\hat{V}(t) \rho_C^0), \quad (\text{E1})$$

where $\hat{V}(t)$ can be viewed as the solution to

$$\frac{d\hat{V}}{dt}(t) = M(\hat{V}(t)), \quad (\text{E2})$$

where the superoperator M is

$$M(\cdot) := i[\hat{H}_C, (\cdot)] - \{\hat{V}, (\cdot)\}. \quad (\text{E3})$$

Using the general solution to ODEs, it follows that $\hat{V}(t) = \exp(Mt)(\hat{V})$. Assuming that M is invertible (we will justify this in appendix E0a) we have

$$\begin{aligned} \int_0^\infty dt \exp(Mt) &= -M^{-1}, & \int_0^\infty dt t \exp(Mt) &= M^{-2}, \\ \int_0^\infty dt t^2 \exp(Mt) &= -2M^{-3}. \end{aligned} \quad (\text{E4})$$

Since integration, trace and matrix multiplication are linear operators, using the equations above we obtain

$$\begin{aligned} \mu &:= \int_0^\infty dt t P_{\text{tick}}(t) = 2 \operatorname{tr}(M^{-2}(\hat{V}) \rho_C^0), \\ \chi &:= \int_0^\infty dt t^2 P_{\text{tick}}(t) = -4 \operatorname{tr}(M^{-3}(\hat{V}) \rho_C^0). \end{aligned} \quad (\text{E5})$$

Equation (E5) are special, in that they provide a means to calculate the first and second moments of the delay function, without having to calculate said function. Further, from $M(\mathbb{1}) = -2\hat{V}$ it follows that $M^{-1}(\hat{V}) = -\frac{1}{2}\mathbb{1}$, ($\mathbb{1}$ being the identity operator), so that we end up with

$$\mu = -\operatorname{tr}(M^{-1}(\mathbb{1}) \rho_C^0), \quad (\text{E6})$$

$$\chi = 2 \operatorname{tr}(M^{-2}(\mathbb{1}) \rho_C^0), \quad (\text{E7})$$

and $\int_0^\infty dt P_{\text{tick}}(t) = \operatorname{tr}(\rho_C^0) = 1$, as expected. This means that the precision can be expressed as

$$R = \frac{1}{\frac{2 \operatorname{tr}(M^{-2}(\mathbb{1}) \rho_C^0)}{-\operatorname{tr}(M^{-1}(\mathbb{1}) \rho_C^0)^2} - 1}. \quad (\text{E8})$$

With this, choosing a matrix representation of M , the problem is reduced to the inversion of a matrix, evaluated on the identity—we have bypassed having to numerically solve for the dynamics of the clockwork.

To solve eq. (E8) we want to find a solution to the two Lyapunov equations

$$M(X) = \mathbb{1}, \quad M(X) = M^{-1}(\mathbb{1}). \quad (\text{E9})$$

The Bartels-Stewart algorithm [22] can solve Lyapunov equations such as these in $O(d^3)$ iterations. In essence, it vectorizes the equation and calculates the Schur decomposition (In fact, we get a little speed up as $M^{-1}(\mathbb{1})$, and $M^{-1}(M^{-1}(\mathbb{1}))$ act on symmetric matrices). In the final step, we need to optimize the precision numerically over the coefficients $\{V_l \geq 0\}_{l=0}^{d-1}$ and ρ_C^0 . From eq. (E8) we can infer that the precision is a rational polynomial in the coefficients $\{V_j\}_{j=0}^{d-1}$ and the coefficients parametrizing the initial clockwork state ρ_C^0 . Therefore, we have finitely many maxima. The numerical optimization algorithm we used picks random seeds, searches, and compares the found local maxima. We constrained the search on $0 \leq V_l \leq d$, as higher coefficients are expected to lead to exponential tails. We used Julia [23], to perform the calculations. The result for the precision is presented in figs. 1 and 5 and shows a d^2 scaling.

a. *Invertibility of M*

One might ask for the general conditions under which M is invertible so that the above equations are well-defined. For this, recall that for an arbitrary matrix C , $M(X) = C$ has a unique solution X , if and only if $M(X) = 0 \Rightarrow X = 0$. From eq. (E3), $M(X) = 0$ reads,

$$(i\hat{H} - \hat{V})X + X(i\hat{H} - \hat{V})^\dagger = 0. \quad (\text{E10})$$

This is known as the continuous Lyapunov equation. One can show by inspecting the implication for the characteristic polynomial³ that it has a unique solution if and only if $\sigma(i\hat{H} - \hat{V}) \cap \sigma(i\hat{H} + \hat{V}) = \emptyset$. Here σ refers to the spectrum of a linear operator. From first order perturbation theory in \hat{V} , we see that the eigenvalues of $i\hat{H} - \hat{V}$ for $n = 0, 1, \dots, d-1$ are

$$\lambda_n = i n - \sum_{k=0}^{d-1} V_k |\langle t_k | n \rangle|^2 = i n - \frac{1}{d} \sum_{k=0}^{d-1} V_k. \quad (\text{E11})$$

Further, all $V_l \geq 0$. Thus, if at least one $V_k > 0$, we expect $\text{Re}(\lambda_l) < 0, l \in \{0, \dots, d-1\}$ and consequently $\lambda_i \neq -\bar{\lambda}_j$ for any two eigenvalues and the condition on the spectrum is satisfied. Physically, negative real parts guaranteed the existence of M^{-1} , which implied $\int_0^\infty dt P_{\text{tick}}(t) = \text{tr}(\rho_C^0) = 1$. Hence, it is equivalent to almost surely observing a tick.

Appendix F: Remarks on the precision of the $d = 2$ clock from virtual qubits of [21]

Firstly, let us observe that the quasi-ideal clock in $d = 2$ for $\rho(0) = |t_1\rangle\langle t_1|$ and $\hat{V} = \frac{1}{\sqrt{2}} |t_0\rangle\langle t_0|$ has a precision of exactly $R = 4$, which is above the classical bound of $R = 2$.

The model suggested in [21] has some similarities with photofluorescence (and therefore can leverage antibunching phenomena). To see this, observe that the environment for the ladder is driving the system via population inversion, described by a negative virtual temperature β_v and is assumed to be perfectly on resonance (or in the RWA limit). We would expect the interaction Hamiltonian

$$H_{int} = g(|0_v\rangle\langle 1_v| \otimes |1_l\rangle\langle 0_l| + h.c.) \quad (\text{F1})$$

to effectively act like

$$H_{int} = g(|1_l\rangle\langle 0_l| + h.c.). \quad (\text{F2})$$

Such a Hamiltonian, however, represents the discrete Fourier transformation of a 2-level system as

$$H = -\frac{\omega}{2} |0\rangle\langle 0| + \frac{\omega}{2} |1\rangle\langle 1| = \frac{1}{2} \begin{pmatrix} 1 & 1 \\ 1 & -1 \end{pmatrix} \begin{pmatrix} -\frac{\omega}{2} & 0 \\ 0 & \frac{\omega}{2} \end{pmatrix} \begin{pmatrix} 1 & 1 \\ 1 & -1 \end{pmatrix} = -\frac{\omega}{2} \begin{pmatrix} 0 & 1 \\ 1 & 0 \end{pmatrix} \quad (\text{F3})$$

$$= -\frac{\omega}{2} (|t_1\rangle\langle t_0| + |t_0\rangle\langle t_1|), \quad (\text{F4})$$

and so $g = -\frac{\omega}{2}$. Consequently, the transition from the lower to the upper level actually behaves like the transition from $|t_0\rangle \rightarrow |t_1\rangle$ with respect to this interaction Hamiltonian. This Hamiltonian does not represent the partial trace over the hot and cold bath and can only serve as an intuition connecting both models. In fluorescence experiments the same principle is used with a laser. Different to a laser, however, the timing in this case is transferred without an explicit electric field in between (that would mediate the timing via a harmonic wave) and is just assumed to exist. To make this analogy on the level of Lindbladians let us recall from [11] that

$$\frac{d\rho_0}{dt} = i \left(\rho_0 H_{\text{eff}}^\dagger - H_{\text{eff}} \rho_0 \right) + \mathcal{L}_h \rho_0 + \mathcal{L}_c \rho_0 \quad (\text{F5})$$

³ The equation is telling us that we can replace left multiplication by $(i\hat{H} - \hat{V})$ with right multiplication by $(-i\hat{H} + \hat{V})$. Thus, using Cayley-Hamilton $0 = q_{(i\hat{H} - \hat{V})}((-i\hat{H} + \hat{V}))X$. By assumption

$q_{(i\hat{H} - \hat{V})}((-i\hat{H} + \hat{V}))$ is non singular, so that $X = 0$.

describes the dynamics on the virtual qubit and the ladder where the effective Hamiltonian is $H_0 + H_{int} - i\Gamma/2 |1_l\rangle\langle 1_l|$. Assuming always decoherent dynamics we have

$$\frac{d\rho_0}{dt} = -i[H_{int}, \rho_0] - \Gamma/2\{\rho_0, |1\rangle\langle 1|\} + \mathcal{L}_h\rho_0 + \mathcal{L}_c\rho_0. \quad (\text{F6})$$

which again does not allow us to trace out hot and cold reservoir as the Hamiltonian term would vanish.

Lastly, let us provide the formula for the partial trace, e.g., $\text{tr}_{h,c}(\exp(-iH_{int}t)\rho_C \otimes \rho_H \otimes \rho_L \exp(iH_{int}t))$, assuming only that the cold and hot qubit are in thermodynamic equilibrium. We obtain

$$\text{tr}_{h,c} \left(\exp(-iH_{int}t)\rho_C \otimes \rho_H \otimes \rho_L \exp(iH_{int}t) \right) \quad (\text{F7})$$

$$= \langle 0_C, 0_H | \left(\exp(-iH_{int}t)\rho_C \otimes \rho_H \otimes \rho_L \exp(iH_{int}t) \right) | 0_C, 0_H \rangle + \quad (\text{F8})$$

$$\langle 1_C, 1_H | \left(\exp(-iH_{int}t)\rho_C \otimes \rho_H \otimes \rho_L \exp(iH_{int}t) \right) | 1_C, 1_H \rangle \quad (\text{F9})$$

$$+ \text{tr}_V \left(\exp(-iH_{int}t)\rho_C \otimes \rho_H \otimes \rho_L \exp(iH_{int}t) \right), \quad (\text{F10})$$

where tr_V is tracing over the virtual qubit states. Because H_{int} acts trivially on non virtual qubit states we get terms proportional to $\rho_L(0)$ on the first two terms. The last term is reduced to a 2-dimensional problem and can be solved since $H_{int}^2 \propto 1$ on the ladder and virtual qubit subspace. In total we obtain

$$\text{tr}_{h,c} \left(\exp(-iH_{int}t)\rho_C \otimes \rho_H \otimes \rho_L \exp(iH_{int}t) \right) = \rho_L(0) \left(\frac{1}{Z_h Z_c} + \frac{e^{-\beta_c E_c} e^{-\beta_h E_h}}{Z_h Z_c} \right) \quad (\text{F11})$$

$$+ |1_L\rangle\langle 1_L| \left(\cos^2(gt) \frac{e^{-\beta_c E_c}}{Z_c Z_h} \langle 1_L | \rho_L(0) | 1_L \rangle + \sin^2(gt) \frac{e^{-\beta_h E_h}}{Z_c Z_h} \langle 0_L | \rho_L(0) | 0_L \rangle \right) \quad (\text{F12})$$

$$+ |0_L\rangle\langle 0_L| \left(\cos^2(gt) \frac{e^{-\beta_h E_h}}{Z_c Z_h} \langle 0_L | \rho_L(0) | 0_L \rangle + \sin^2(gt) \frac{e^{-\beta_c E_c}}{Z_c Z_h} \langle 1_L | \rho_L(0) | 1_L \rangle \right). \quad (\text{F13})$$

This form clearly reveals the effect of a varying initial state. If the probability of ticking is coupled to occupying the top state and we start the dynamics in the ground state $\rho_L(0) = |0\rangle\langle 0|$ the probability to occupy the top state is

$$P_{top}(t) = \text{tr}_l (|1_l\rangle\langle 1_l| \rho_l(t)) = \sin^2(gt) \frac{e^{-\beta_h E_h}}{Z_c Z_h}. \quad (\text{F14})$$

Coupling this to a photon field, the way it was done in [21], then yields

$$P_{tick}(t) = c \frac{e^{-\beta_h E_h}}{Z_c Z_h} \sin^2(gt) \exp\left(-\frac{c}{2} \frac{e^{-\beta_h E_h}}{Z_c Z_h} t\right) \exp\left(\frac{c}{2} \frac{e^{-\beta_h E_h}}{Z_c Z_h} \frac{\sin(gt) \cos(gt)}{g}\right). \quad (\text{F15})$$

Lastly, let us compare the $d = 2$ classical clock without virtual qubits with the quasi-ideal clock in $d = 2$. The $d = 2$ classical clock utilizes a single excitation and is supposed to decay thereafter. The probability of ticking being te^{-t} . Now, the virtual qubit as well as the quasi-ideal clock allow for oscillation, that is, we have a finite probability of going back to the ground state (no selection rule). Thus, in $d = 2$ we get oscillations, which is reflected in the appearance of the $\cos(gt)$ and $\sin(gt)$ terms multiplying the exponential in eq. (F15). The comparison with lasers shows that the virtual qubit case satisfies this. Finally, the virtual qubit case fundamentally reflects an 8-dimensional case, as the interaction with the ladder is providing the timing (meaning that if we were to make the interaction between the virtual qubit and ladder Markovian, the clock would not function). It was this extra dimension that allowed us to tweak the Hamiltonian to mimic a discrete Fourier transformation. To avoid this extra dimension, we could leave the Hamiltonian diagonal but instead utilize a different decay mechanism and initial state (Fourier transform them instead). So we deduce that the key pieces are allowing oscillations, having a non-diagonal decay channel and a non-diagonal initial state.

Appendix G: Analytical expression for the Entropy production for the $d = 2$ quasi-ideal thermal clock

In the following we provide the relevant calculation for the Entropy, provided by Eq. 20 for the case of $d = 2$, $V_0 = 0$, $\rho(0) = |t_0\rangle\langle t_0|$. We work here in a three level system as the states $|0\rangle, |1\rangle$ are decaying to the state $|u\rangle$. We can

assume a spectrum of $(-\omega_0, 0, \omega)$ for the states $|u\rangle, |0\rangle, |1\rangle$. The thermal state will be reached due to equilibration with the photon bath to be $\exp\{-\beta H\}/Z$, so that the $\log(\rho_t h) = -\beta H$ can be used. To calculate the dynamics, we will assume $H = |1\rangle, \hat{V} = V_1 |t_1\rangle\langle t_1|$ as the dynamics conditioned on not-ticking is entirely in the two level $|0\rangle, |1\rangle$ subspace. The final solution is then obtained by scaling $t \rightarrow t\omega, V_1 \rightarrow V_1(1 + N)/\omega$, where N is the occupation number of the bath. This factor enters, because we have the possibility of absorption. However, the photons being absorbed also produce a tick, so that conditioning on no-tick also eliminates the absorbing part of the dynamics. We start by decomposing in to the Pauli-matrices $\sigma_0, \sigma_1, \sigma_2, \sigma_3$ and work in the time-basis.

$$H = \frac{1}{2}(\sigma_0 - \sigma_1), \quad V = \frac{V_1}{2}(\sigma_0 - \sigma_3), \quad \rho(0) = \frac{1}{2}(\sigma_3 + \sigma_0) \quad (\text{G1})$$

Then $\exp(-iHt - Vt) = e^{-it/2} e^{-V_1 t/2} \left(\cosh\left(t \frac{\sqrt{V_1^2 - 1}}{2}\right) \sigma_0 + \frac{i \sinh\left(t \frac{\sqrt{V_1^2 - 1}}{2}\right)}{\sqrt{V_1^2 - 1}} \sigma_1 + \frac{V_1}{\sqrt{V_1^2 - 1}} \sigma_3 \right)$. Now we can calculate $\exp(-iHt - Vt) * \rho_C^0 * \exp(iHt - Vt)$. We decompose the result into Pauli-matrices too

$$\exp(-iHt - Vt) \rho_C^0 \exp(iHt - Vt) = a_0(t) \sigma_0 + a_1(t) \sigma_1 + a_2(t) \sigma_2 + a_3(t) \sigma_3 \quad (\text{G2})$$

and obtain

$$a_0(t) = e^{-V_1 t} \left(\frac{\cosh^2\left(t \frac{\sqrt{V_1^2 - 1}}{2}\right)}{2} + \frac{V_1 \cosh\left(t \frac{\sqrt{V_1^2 - 1}}{2}\right)}{2\sqrt{V_1^2 - 1}} + \frac{V_1}{2\sqrt{V_1^2 - 1}} \cosh\left(t \frac{\sqrt{V_1^2 - 1}}{2}\right) + \frac{V_1^2}{2(V_1^2 - 1)} + \frac{\sinh^2\left(t \frac{\sqrt{V_1^2 - 1}}{2}\right)}{2(V_1^2 - 1)} \right) \quad (\text{G3})$$

$$a_1(t) = 0 \quad (\text{G4})$$

$$a_2(t) = e^{-V_1 t} \left(\frac{\sinh\left(t \frac{\sqrt{V_1^2 - 1}}{2}\right) \cosh\left(t \frac{\sqrt{V_1^2 - 1}}{2}\right)}{\sqrt{V_1^2 - 1}} + \frac{\sinh\left(t \frac{\sqrt{V_1^2 - 1}}{2}\right) V_1}{(V_1^2 - 1)} \right) \quad (\text{G5})$$

$$a_3(t) = e^{-V_1 t} \left(\frac{\cosh^2\left(t \frac{\sqrt{V_1^2 - 1}}{2}\right)}{2} + \frac{V_1 \cosh\left(t \frac{\sqrt{V_1^2 - 1}}{2}\right)}{2\sqrt{V_1^2 - 1}} + \frac{V_1}{2\sqrt{V_1^2 - 1}} \cosh\left(t \frac{\sqrt{V_1^2 - 1}}{2}\right) + \frac{V_1^2}{2(V_1^2 - 1)} - \frac{\sinh^2\left(t \frac{\sqrt{V_1^2 - 1}}{2}\right)}{2(V_1^2 - 1)} \right) \quad (\text{G6})$$

By the property of the Pauli-matrices, we have that $\text{tr}(\exp(-iHt - Vt) \rho_C^0 \exp(iHt - Vt)) = 2a_0(t)$. Then, we need to calculate how the non-tick Lindbladian acts on the Pauli Matrices. Due to the decomposition of H, V this means

$$\mathcal{L}(\rho) = -\frac{i}{2}[(\sigma_0 - \sigma_1), \rho] - \frac{V_1}{2}\{\sigma_0 - \sigma_3, \rho\} \quad (\text{G7})$$

$$\mathcal{L}(\sigma_0) = V_1(\sigma_3 - \sigma_0) \quad (\text{G8})$$

$$\mathcal{L}(\sigma_1) = -2V_1 \sigma_1 \quad (\text{G9})$$

$$\mathcal{L}(\sigma_2) = -\sigma_3 - V_1 \sigma_2 \quad (\text{G10})$$

$$\mathcal{L}(\sigma_3) = \sigma_2 + V_1(\sigma_0 - \sigma_3). \quad (\text{G11})$$

Multiplying from the left with H and taking the trace yields

$$\text{tr}(H \mathcal{L}(\sigma_0)) = -V_1 \quad (\text{G12})$$

$$\text{tr}(H \mathcal{L}(\sigma_1)) = 2V_1 \quad (\text{G13})$$

$$\text{tr}(H \mathcal{L}(\sigma_2)) = 0 \quad (\text{G14})$$

$$\text{tr}(H \mathcal{L}(\sigma_3)) = V_1 \quad (\text{G15})$$

Finally, the probability of ticking reads

$$P(t) = 2 \text{tr}(\hat{V} \rho(t)) = V_1(\text{tr}(\rho(t)) - \text{tr}(\sigma_3 \rho(t))) = 2V_1(a_0(t) - a_3(t)) \quad (\text{G16})$$

$$= \frac{2V_1}{V_1^2 - 1} e^{-V_1 t} \sinh^2\left(t \frac{\sqrt{V_1^2 - 1}}{2}\right). \quad (\text{G17})$$

In total, using linearity we obtain

$$\Delta S_{\text{tick}} = -\beta \int_0^\infty dt P(t) \int_0^t ds \text{tr}(H\mathcal{L}(\rho(s))/\text{tr}(\rho(s))) \quad (\text{G18})$$

$$= -\beta \int_0^\infty dt P(t) \int_0^t ds (-V_1 a_0(s) + 2V_1 a_1(s) + V_1 a_3(s))/a_0(s) \quad (\text{G19})$$

$$= \beta \int_0^\infty dt P(t) \int_0^t ds \frac{P(s)}{2a_0(s)}. \quad (\text{G20})$$

Recall that we need to make the substitution $t, s \rightarrow \omega t, \omega s$, $V_1 \rightarrow V_1/\omega$.

-
- [1] C. R. S. Williams, J. C. Salevan, X. Li, R. Roy, and T. E. Murphy, Fast physical random number generator using amplified spontaneous emission, *Opt. Express* **18**, 23584 (2010).
- [2] M. P. Woods, R. Silva, G. Pütz, S. Stupar, and R. Renner, Quantum clocks are more accurate than classical ones, *PRX Quantum* **3**, 010319 (2022).
- [3] R. R. Yuxiang Yang, Ultimate limit on time signal generation, <https://arxiv.org/abs/2004.07857> (2020).
- [4] M. P. Woods, Autonomous ticking clocks from axiomatic principles, *Quantum* **5**, 381 (2021).
- [5] M. P. Woods, R. Silva, and J. Oppenheim, Autonomous quantum machines and finite-sized clocks, *Annales Henri Poincaré* **20**, 125 (2019).
- [6] F. Meier, E. Schwarzahans, P. Erker, and M. Huber, Fundamental accuracy-resolution trade-off for timekeeping devices (2023), arXiv:2301.05173.
- [7] N. W. Ashcroft and N. D. Mermin, *Solid State Physics* (Holt-Saunders, 1976).
- [8] H. Breuer, F. Petruccione, and S. Petruccione, *The Theory of Open Quantum Systems* (Oxford University Press, 2002).
- [9] H. Spohn, Entropy production for quantum dynamical semigroups, *Journal of Mathematical Physics* **19**, 1227 (1978), <https://doi.org/10.1063/1.523789>.
- [10] J. Arnold, Entropy production in ticking clocks (2021), Supervisor: M. Woods.
- [11] P. Erker, M. T. Mitchison, R. Silva, M. P. Woods, N. Brunner, and M. Huber, Autonomous quantum clocks: Does thermodynamics limit our ability to measure time?, *Phys. Rev. X* **7**, 031022 (2017).
- [12] G. J. Milburn, The thermodynamics of clocks, *Contemporary Physics* **61**, 69 (2020).
- [13] A. N. Pearson, Y. Guryanova, P. Erker, E. A. Laird, G. A. D. Briggs, M. Huber, and N. Ares, Measuring the thermodynamic cost of timekeeping, *Phys. Rev. X* **11**, 021029 (2021).
- [14] X. He, P. Pakkiam, A. Gangat, G. Milburn, and A. Fedorov, Measurement driven quantum clock implemented with a superconducting qubit (2022), arXiv:2207.11043.
- [15] A. D. Greentree, J. Koch, and J. Larson, Fifty years of Jaynes–Cummings physics, *Journal of Physics B: Atomic, Molecular and Optical Physics* **46**, 220201 (2013).
- [16] M. Gross and S. Haroche, Superradiance: An essay on the theory of collective spontaneous emission, *Physics Reports* **93**, 301 (1982).
- [17] J. Schelter, P. Recher, and B. Trauzettel, The Aharonov–Bohm effect in graphene rings, *Solid State Communications* **152**, 1411 (2012), exploring Graphene, *Recent Research Advances*.
- [18] F. Brange, A. Schmidt, J. C. Bayer, T. Wagner, C. Flindt, and R. J. Haug, Controlled emission time statistics of a dynamic single-electron transistor, *Science Advances* **7**, 10.1126/sciadv.abe0793 (2021).
- [19] S. F. H. Angel Rivas, *Open quantum systems - an introduction*, SpringerBriefs in Physics (2012).
- [20] F. P. Heinz-Peter Breuer, *The theory of open quantum systems*, Oxford University Press 10.1093/acprof:oso/9780199213900.001.0001 (2007).
- [21] E. Schwarzahans, M. P. E. Lock, P. Erker, N. Friis, and M. Huber, Autonomous temporal probability concentration: Clockworks and the second law of thermodynamics, *Phys. Rev. X* **11**, 011046 (2021).
- [22] R. H. Bartels and G. W. Stewart, Solution of the matrix equation $ax + xb = c$ [f4], *Commun. ACM* **15**, 820–826 (1972).
- [23] J. Bezanson, A. Edelman, S. Karpinski, and V. B. Shah, Julia: A fresh approach to numerical computing, *SIAM Review* **59**, 65 (2017).